Int J Earth Sci (Geol Rundsch) (2017) 106:1963–1989
DOI 10.1007/s00531-016-1402-4

ORIGINAL PAPER

U–Pb ages, geochemistry, C–O–Nd–Sr–Hf isotopes and petrogenesis of the Catalão II carbonatitic complex (Alto Paranaíba Igneous Province, Brazil): implications for regional-scale heterogeneities in the Brazilian carbonatite associations

Vincenza Guarino[1] · Fu-Yuan Wu[2] · Leone Melluso[1] · Celso de Barros Gomes[3] · Colombo Celso Gaeta Tassinari[3] · Excelso Ruberti[3] · Mauro Brilli[4]

Received: 14 March 2016 / Accepted: 18 September 2016 / Published online: 30 September 2016

Abstract The Catalão II carbonatitic complex is part of the Alto Paranaíba Igneous Province (APIP), central Brazil, close to the Catalão I complex. Drill-hole sampling and detailed mineralogical and geochemical study point out the existence of ultramafic lamprophyres (phlogopite-picrites), calciocarbonatites, ferrocarbonatites, magnetitites, apatitites, phlogopitites and fenites, most of them of cumulitic origin. U–Pb data have constrained the age of Catalão I carbonatitic complex between 78 ± 1 and 81 ± 4 Ma. The initial strontium, neodymium and hafnium isotopic data of Catalão II ($^{87}Sr/^{86}Sr_i$ = 0.70503–0.70599; εNd_i = −6.8 to −4.7; $^{176}Hf/^{177}Hf$ = 0.28248–0.28249; εHf_i = −10.33 to −10.8) are similar to the isotopic composition of the Catalão I complex and fall within the field of APIP kimberlites, kamafugites and phlogopite-picrites, indicating the provenance from an old lithospheric mantle source. Carbon isotopic data for Catalão II carbonatites ($\delta^{13}C$ = −6.35 to −5.68 ‰) confirm the mantle origin of the carbon for these rocks. The origin of Catalão II cumulitic rocks is thought to be caused by differential settling of the heavy phases (magnetite, apatite, pyrochlore and sulphides) in a magma chamber repeatedly filled by carbonatitic/ferrocarbonatitic liquids (*s.l.*). The Sr–Nd isotopic composition of the Catalão II rocks matches those of APIP rocks and is markedly different from the isotopic features of alkaline-carbonatitic complexes in the southernmost Brazil. The differences are also observed in the lithologies and the magmatic affinity of the igneous rocks found in the two areas, thus demonstrating the existence of regional-scale heterogeneity in the mantle sources underneath the Brazilian platform.

Keywords U–Pb baddeleyite geochronology · Lu–Hf isotopes · Sr–Nd isotopes · Carbonatites · Catalão II · Brazil

Introduction

In Brazil, 22 alkaline complexes containing carbonatites have been identified, associated with alkaline ultramafic intrusive rocks and phonolites/nephelinites/melilitites (Morbidelli et al. 1995; Woolley and Kjarsgaard 2008a, b). These complexes have been emplaced in and around the Paraná Basin during an extended time period (Fig. 1). The Iporá province was emplaced 98 Ma ago along the N–NE border; the Alto Paranaíba Igneous Province (hereafter APIP; Fig. 1) was emplaced at 70–98 Ma along the NE border; the São Paulo-Paraná province was emplaced 101–143 Ma ago along the SE border; the Santa Catarina Province was emplaced 68–132 Ma ago along the S–SE border. The Chiriguelo and Cerro Sabatini complexes (Paraguay) were emplaced at ~125 Ma along the south-western border of the Paraná Basin.

Electronic supplementary material The online version of this article (doi:10.1007/s00531-016-1402-4) contains supplementary material, which is available to authorized users.

✉ Vincenza Guarino
vincenza.guarino@unina.it

[1] Dipartimento di Scienze della Terra, dell'Ambiente e delle Risorse, Università di Napoli Federico II, Via Mezzocannone 8, 80134 Naples, Italy

[2] State Key Laboratory of Lithospheric Evolution, Institute of Geology and Geophysics, Chinese Academy of Sciences, Beijing 100029, China

[3] Instituto de Geociências, Universidade de São Paulo, Rua do Lago 562, 05508-080 São Paulo, Brazil

[4] Istituto di Geologia Ambientale e Geoingegneria (IGAG) CNR, Area della Ricerca RM1, via Salaria km 29.300, Monterotondo Scalo, 00016 Rome, Italy

Several petrogenetic mechanisms are hypothesized for the genesis of carbonatitic rocks: (a) liquid immiscibility between silicate and carbonate liquids (Lee and Wyllie 1996, 1997a, b; Lee and Wyllie 1998; Wyllie and Lee 1998); (b) prolonged fractional crystallization of a carbonate-rich silicatic magma (Otto and Wyllie 1993; Lee and Wyllie 1994); and (c) low-degree melting of recycled oceanic crust in the form of a carbonated eclogite or carbonated metapelite (Barker 1996; Hoernle et al. 2002; Grassi and Schmidt 2010). In these processes, carbonate-rich and silicate-rich conjugate liquids should be in geochemical and isotopic equilibrium.

Many authors link the genesis of carbonatites to the presence of mantle plumes (Bell 2001; Bell and Tilton 2001, 2002; Dunworth and Bell 2001; Bizzarro et al. 2002; Hoernle et al. 2002; Bell and Rukhlov 2004; Kogarko 2006; Bell and Simonetti 2010). Barker (1996) concludes that carbonatites are the ultimate product of recycled oceanic crust, because both $^{87}Sr/^{86}Sr$ and C isotope ratios of carbonatites are consistent with limestone input into the mantle. Gibson et al. (1995), Thompson et al. (1998) and Bulanova et al. (2010) hypothesized the existence of a track of igneous activity, related to the passage of the South American platform over a fixed hotspot, from Goiás (90–88 Ma) to Serra do Mar (80–55 Ma).

The Catalão II carbonatitic complex is one of the largest intrusions that form the province. It is located in the north-western part of the APIP (Fig. 1) in Brazil, which is one of the largest ultrapotassic/carbonatitic/kimberlitic provinces in the world. This paper reports a new dataset of in situ U–Pb ages, mineral chemistry, bulk-rock major, trace element and isotopic data ($^{87}Sr/^{86}Sr$; $^{143}Nd/^{144}Nd$; $^{176}Hf/^{177}Hf$; $\delta^{18}O$; $\delta^{13}C$) on the lithotypes that form this intrusion, together with new data for the nearby Catalão I complex, which is better known from the papers of Cordeiro et al. (2010, 2011a, b). The aim is to constrain the petrogenesis of the Catalão II complex, to highlight its relationships with the other rocks of the APIP and to characterize its mantle source in the light of the regional variations of the alkaline-carbonatitic magmatism in southern Brazil.

Geological setting

The APIP is one of the largest ultrapotassic/kamafugitic provinces of the world and extends over ~20,000 km^2 between the São Francisco Craton and the north-eastern border of the Paraná Basin (south-eastern Brazil) (Fig. 1). It is located across SE Minas Gerais and SW Góias on a Late Precambrian mobile belt (the Brasilia Belt), between the NE margin of the Paraná Basin and the SW margin of the São Francisco Craton (Almeida et al. 2000; D'Agrella-Filho et al. 2011; Peucat et al. 2011 and references therein). The Late Cretaceous–Cenozoic igneous rocks of south-eastern Brazil are aligned along two main trends: the first is oriented along NW–SE (APIP), whereas the second trends are along W–E (Serra do Mar Igneous Province). The APIP magmatism occurred during the Late Cretaceous (~91–71 Ma; Gibson et al. 1995; Sgarbi et al. 2004; Gomes and Comin-Chiaramonti 2005; Carlson et al. 2007; Guarino et al. 2013) in and on top of Proterozoic metamorphosed crustal sequences (quartzite and micaschistes) of the Brasilia mobile belt (Almeida et al. 2000). This belt represents a strongly folded terrane (with ages of peak metamorphism around 790 and 630–610 Ma; Pimentel et al. 2000) forming the western boundary of the São Francisco Craton. The mafic potassic to ultrapotassic magmatism of the APIP consists of plugs, dykes, lava flows, pipes, pyroclastic deposits and plutonic complexes. The identified rocks are kamafugites, kimberlites, lamprophyres and carbonatites (Gibson et al. 1995; Carlson et al. 1996; Morbidelli et al. 1997; Brod et al. 2000; Araújo et al. 2001; Read et al. 2004; Gomes and Comin-Chiaramonti 2005; Melluso et al. 2008; Guarino et al. 2013), emplaced as lava flows (e.g. Presidente Olegario), heavily altered pyroclastic successions (Coromandel), hypabyssal facies (e.g. Pântano, Três Ranchos, Osmar, Limeira, Indaiá) and dunitic/pyroxenitic/carbonatitic/phoscoritic intrusions (e.g. Catalão I, Catalão II, Araxá, Tapira and Salitre).

The Catalão II and Catalão I complexes are located in the APIP, in the south-eastern part of Goiás and the western part of Minas Gerais. They are 10 km apart from each other and located 20 and 15 km north-east of the town of Catalão, respectively. The complexes are covered by a lateritic soil, about 50 m thick at Catalão II and up to 25 m thick at Catalão I (Guimarães and Weiss 2013; Rocha et al. 2001).

The *Catalão II complex* (18°02′ S, 47°52′ W, 5 × 2.7 km; Fig. 2) intruded the Araxá Group (quartzites, schists and phyllites) of the Late Proterozoic Brasília Belt and is situated along a NW–SE lineament that controlled the emplacement of Cretaceous alkaline rocks of the APIP (Biondi 2005). The Catalão II complex consists of two magmatic pipes, opposed to the Catalão I complex, which exhibits a single-dome structure. The two pipes have a circular shape of 14 km^2 and are about 2 km apart (Fig. 2) and consist of a complex crosscutting relationships of dykes, veins and alkaline igneous bodies (Machado 1991; Rocha et al. 2001). The Catalão II complex is known for the alteration of magmatic pyrochlore into secondary phases during supergene alteration processes in the alteration cover and the related mineralization (Rocha et al. 2001; Guimarães and Weiss 2013).

The *Catalão I complex* (18°08′ S, 47°50′ W) has a circular dome shape 27 km^2 in size. Cordeiro et al. (2010, 2011a, b) identified dolomite carbonatite and phoscorite-series rocks and summarized the resources, geology and

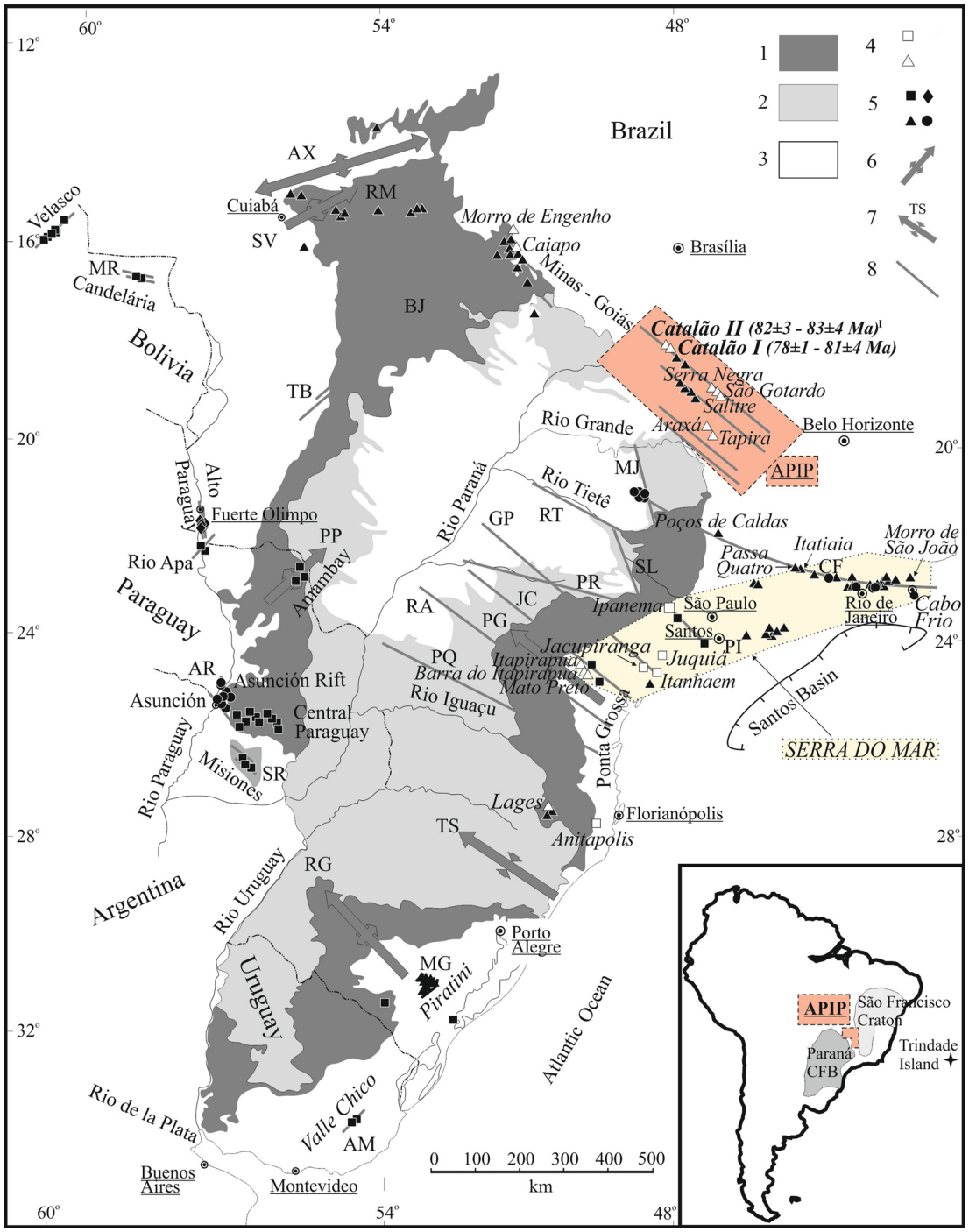

Fig. 1 Location and U–Pb ages of the Catalão II ([I] Guarino et al. 2013) and Catalão I (this study) alkaline-carbonatite complexes in Brazil. The alkaline provinces of the central-south-eastern region of the Brazilian Platform and their relationships to major structural features are also shown (after Riccomini et al. 2005; Melluso et al. 2016): *1* Late Ordovician to Early Cretaceous Paraná Basin; *2* Early Cretaceous tholeiitic lava flows; *3* Late Cretaceous Bauru Basin; *4* alkaline complexes associated with carbonatites and *5* alkaline complexes without associated carbonatites (age: *diamonds*, Permian–Triassic; *squares*, Early Cretaceous; *triangles*, Late Cretaceous; *circles*, Palaeogene); *6* axes of main arcs (AX, Alto Xingu; SV, São Vicente; BJ, Bom Jardim de Goiás; PG, Ponta Grossa; RG, Rio Grande; PP, Ponta Porã); *7* Torres Syncline; and *8* major fracture zones, in part deep lithospheric faults (*Rifts*: *MR* Mercedes; *RM* Rio das Mortes; *MG* Moirão; *SR* Santa Rosa; *AR* Asunción; *Lineaments*: *TB* Transbrasiliano; *MJ* Moji-Guaçu; *CF* Cabo Frio; *RT* Rio Tietê; *SL* São Carlos-Leme; *PR* Paranapanema; *PI* Piedade; *GP* Guapiara; *JC* São Jerônimo-Curiúva; *RA* Rio Alonzo; *PQ* Rio Piquiri; *AM* Santa Lucia-Aiguá-Merin). *Inset* the *inset* shows the location of the Paraná Basin CFB (Continental Flood Basalts), the São Francisco Craton, Trindade Island and the APIP

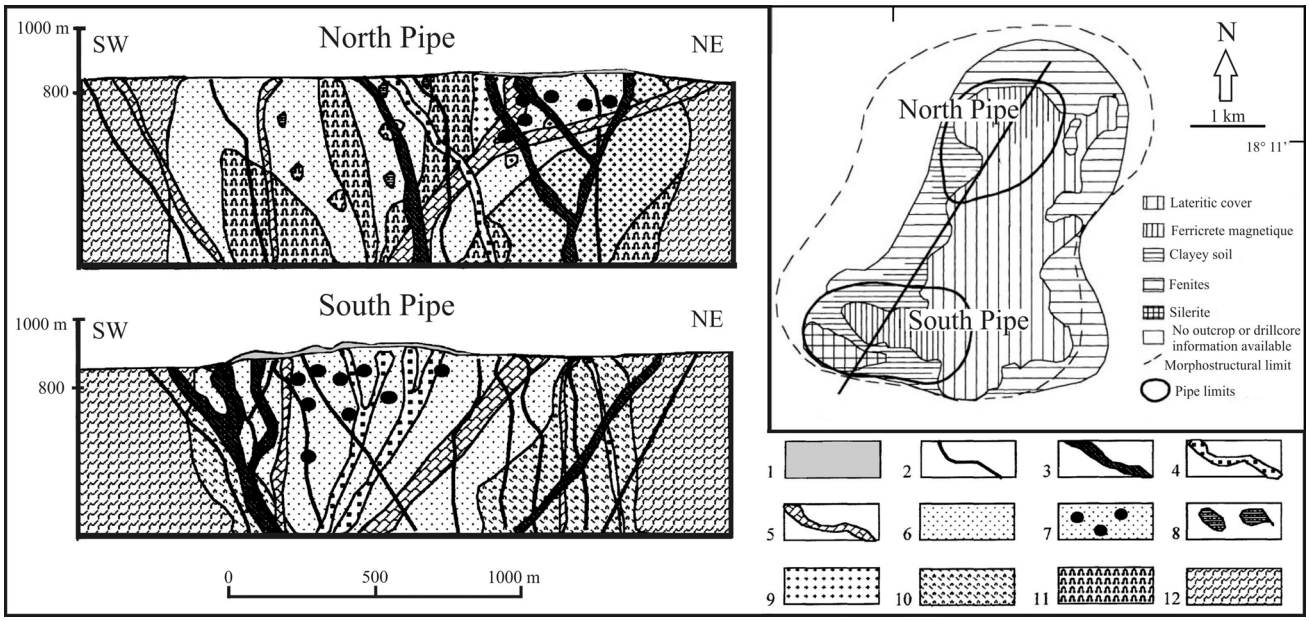

Fig. 2 Schematic map of the Catalão II alkaline-carbonatitic complex (modified after Rocha et al. 2001). *1* residual magnetitite blocks; *2* lamprophyres; *3–6* carbonatites; *7* pyrochlore-rich carbonatites; *8* apatitite/magnetitite; *9* syenites; *10* phlogopitite; *11* clinopyroxenites; and *12* Proterozoic metamorphosed crustal sequences (quartzite and micaschistes)

pyrochlore chemistry. These authors suggested a common parental magma for phoscorites and carbonatites based on the REE patterns and Sr–Nd isotopes. Furthermore, the C–O isotopic systematic indicates that dolomite carbonatites underwent several post-magmatic events, such as magmatic fractionation (Rayleigh and degassing) and three-fluid fractionation (fluid degassing, H_2O percolation and CO_2–H_2O fluid percolation). Mantovani et al. (2016) estimated the shape and volume for the carbonatite body of about 1.99 km^3 of Catalão I complex utilizing gravity and magnetic data. They also pointed out the presence of fresh rocks below 500 m depth.

Drill-core samples and analytical techniques

The samples of this study have been obtained through drill cores crosscutting the lateritic soil: C3B2(A) and C3B1(B) boreholes at Catalão II, from south and north pipes, respectively, and F72, 3E19 N and 49E33 N boreholes at Catalão I.

The investigated lithologies (lamprophyres, carbonatites, phlogopite-, apatite- and magnetite-rich rocks) are listed in all tables according to their depth in the boreholes. A representative set of 19 samples from Catalão II, and eight from Catalão I, were selected, cut and then crushed using a low-blank agate mortars. The ICP-OES (inductively coupled plasma–optical emission system) and ICP-MS (inductively coupled plasma–mass spectrometer) methods at the Activation Laboratories (Canada), on the powder of these samples, have been used to obtain major element oxides, lanthanide rare earths (REE) and other trace elements (Table 1). The thin sections of the Catalão II and Catalão I rocks were observed in polarized light microscopy, through a Leitz Laborlux 12 POL microscope, to identify the mineralogical phases. The modal analysis is based on 3000 points and was carried out with Leica QWin software equipped with a Leica DFC280 camera (Supplementary Table 1). A JEOL JSM-5310 electron microscope equipped with an INCAx-act EDS detector at University of Napoli Federico II is used to obtain the chemical composition of mineralogical phases (carbonates, Fe–Ti oxides, apatite, pyrochlore, phlogopite, olivine, perovskite, garnet, amphibole and alkali feldspar) on polished thin sections (full details in Melluso et al. 2010, 2014, 2016). A Cameca SX50 electron microprobe equipped with five spectrometers at IGAG–CNR (Rome) was also used to obtain additional chemical composition of mineral phases (phlogopite, carbonate and pyrochlore). The bulk-rock Sr and Nd isotope analyses were performed at the Geochronological Research Center, University of São Paulo, with a VG354 Micromass multicollector mass spectrometer (analytical details in Sato et al. 1995). Stable isotope analyses were obtained at the Istituto di Geologia Ambientale e Geoingegneria (CNR), Rome, using a Finnigan Delta plus mass spectrometer for oxygen isotope analyses on calcite and other minerals and a Finnigan MAT 252 mass spectrometer for carbon isotope analyses (Rossetti et al. 2007). In situ U–Pb age determinations

Table 1 Major (wt %) and trace elements (ppm) concentrations of the Catalão II and Catalão I rocks

Site	Rock	Bore-hole no.	Depth below ground-level	Sample	SiO_2 (wt %)	TiO_2	Al_2O_3	$Fe_2O_{3(T)}$	MnO	MgO	CaO	Na_2O	K_2O	P_2O_5	LOI	Total	Sc (ppm)	Be	V	Ba	Sr	Y	Zr	Cr	Co	Ni	Cu	Zn	Ga	Ge	As	Rb
Catalão II	CaCc	C3B2 (A)	79.2	C2A2	4.02	0.05	0.06	2.54	0.10	2.82	46.49	0.10	1.10	1.08	38.52	96.9	4	1	8	5305	>10,000	34	17	<20	7	<20	80	<30	4	1	<5	51
Catalão II	Syenite	C3B2 (A)	109.7	C2A6	44.67	0.51	4.65	10.41	0.22	14.18	10.00	2.08	5.82	2.34	4.77	99.6	29	5	209	810	1089	17	117	720	41	250	10	110	8	2	<5	173
Catalão II	Phl-Picrite	C3B2 (A)	137.8	C2A8	30.68	6.18	3.90	15.63	0.19	16.57	10.17	0.26	3.27	2.79	10.31	100.0	27	5	216	3874	2333	40	792	830	60	310	120	160	16	2	5	218
Catalão II	Phl-Picrite	C3B2 (A)	161.2	C2A10	29.26	6.38	4.69	15.66	0.23	14.36	11.17	0.28	4.56	3.35	9.20	99.2	31	5	178	4257	2184	44	1032	850	51	160	130	140	19	2	<5	259
Catalão II	Phlogopi-tite	C3B2 (A)	165.2	C2A11	30.03	0.83	5.45	15.82	0.14	17.73	11.21	0.25	7.11	3.29	8.05	99.9	9	4	314	978	2239	21	1158	130	47	60	70	90	13	2	<5	321
Catalão II	CaCc	C3B2 (A)	271.2	C2A15	0.32	0.03	0.06	0.40	0.10	1.74	47.17	0.03	0.10	0.07	41.13	91.2	10	<1	23	22370	>10,000	60	16	<20	<1	<20	80	<30	6	1	<5	<2
Catalão II	CaCc	C3B2 (A)	287.0	C2A17	0.31	0.03	0.03	0.91	0.05	0.57	53.13	0.06	0.09	0.08	41.90	97.2	3	1	11	2702	>10,000	27	11	20	5	20	210	30	3	1	5	5
Catalão II	Phl-Picrite	C3B2 (A)	290.1	C2A18	30.24	4.64	4.48	12.41	0.18	18.67	11.19	0.14	4.48	1.69	10.89	99.0	23	4	172	3440	4453	28	556	1040	56	360	70	180	15	1	5	212
Catalão II	CaCc	C3B2 (A)	314.0	C2A19	3.41	0.17	0.05	4.42	0.09	2.47	46.45	0.06	0.80	1.55	35.42	94.9	5	2	32	6635	>10,000	32	82	20	30	20	210	30	4	1	5	52
Catalão II	CaCc	C3B2 (A)	320.0	C2A20	1.41	0.02	0.03	2.09	0.07	1.08	50.68	0.09	0.32	1.03	38.91	95.7	5	1	10	4028	>10,000	36	18	20	23	20	110	30	4	1	5	16
Catalão II	CaCc	C3B2 (A)	324.8	C2A21	4.32	0.43	0.04	2.95	0.08	2.85	47.47	0.09	1.08	3.26	35.32	97.9	6	2	17	2933	>10,000	32	25	20	5	20	90	30	4	1	5	71
Catalão II	Magneti-tite	C3B2 (A)	353.1	C2A24	6.75	9.91	0.15	63.26	0.68	6.59	4.61	0.13	1.76	2.16	1.98	98.0	36	7	1111	873	1780	31	1095	<20	93	130	330	360	8	3	7	100
Catalão II	Apatitite	C3B1 (B)	127.7	C2B3	10.91	2.12	0.38	32.04	0.16	6.82	24.14	0.29	2.15	16.73	3.90	99.6	10	8	1223	618	3620	62	842	100	41	50	10	140	12	3	6	120
Catalão II	CaCc	C3B1 (B)	308.5	C2B17	0.21	–	0.01	0.23	0.07	0.56	53.56	0.11	0.14	0.25	42.78	97.9	4	1	5	4531	>10,000	28	6	20	1	20	10	30	3	1	5	4
Catalão II	FeCc	C3B1 (B)	312.9	C2B18	14.89	0.12	0.28	8.42	0.09	8.12	32.99	0.14	3.42	14.79	13.91	97.2	4	9	31	1430	8377	56	15	20	6	20	20	100	6	2	5	233
Catalão II	CaCc	C3B1 (B)	328.5	C2B19	3.46	0.88	0.03	5.16	0.11	2.51	46.02	0.06	0.84	2.71	35.11	96.9	5	1	81	3036	>10,000	27	28	20	5	20	70	50	4	1	5	56
Catalão II	CaCc	C3B1 (B)	354.0	C2B22	1.10	0.04	0.05	1.31	0.27	1.03	50.23	0.05	0.19	0.67	41.50	96.4	5	<1	12	3483	>10,000	104	12	<20	<1	<20	<10	<30	6	1	<5	<2
Catalão II	Phl-Picrite	C3B1 (B)	368.8	C2B23	31.74	6.47	4.05	15.41	0.24	15.10	7.96	0.35	4.53	1.68	10.08	97.6	29	5	179	6234	4077	31	842	270	51	190	130	120	15	2	<5	240
Catalão II	FeCc	C3B1 (B)	400.0	C2B24	8.77	0.71	1.44	8.88	0.14	2.33	43.06	0.16	0.64	1.31	31.91	99.3	5	2	108	2606	>10,000	36	482	<20	14	<20	100	50	10	1	<5	52
Catalão I	Magneti-tite	F72	100.0	C1A5	6.47	0.91	0.11	63.89	0.41	12.76	7.00	0.07	0.44	2.22	5.52	99.8	75	3	701	400	2429	9	1636	<20	100	<20	210	290	12	3	<5	25
Catalão I	MgCc	3E 19 N	175.0	C1B10	3.75	0.02	0.09	1.32	0.49	29.73	11.87	0.03	0.05	1.60	42.14	91.1	56	3	28	19610	>10,000	204	236	20	6	20	10	580	56	7	21	2
Catalão I	MgCc	49E 33 N	114.8	C1C2	1.24	–	0.12	3.08	0.30	20.36	25.43	0.01	0.01	3.12	38.95	92.6	51	3	20	17990	>10,000	114	69	20	99	20	10	50	125	14	38	2

Table 1 continued

Site	Rock	Borehole no.	Depth below ground-level	Sample	SiO_2 (wt %)	TiO_2	Al_2O_3	$Fe_2O_{3(T)}$	MnO	MgO	CaO	Na_2O	K_2O	P_2O_5	LOI	Total	Sc (ppm)	Be	V	Ba	Sr	Y	Zr	Cr	Co	Ni	Cu	Zn	Ga	Ge	As	Rb
Catalão I	MgCc	49E 33 N	130.0	C1C4	0.64	0.02	0.05	2.00	0.37	19.26	25.41	0.07	0.01	1.04	41.95	90.8	12	1	16	52300	>10,000	31	21	20	3	20	10	40	8	1	5	2
Catalão I	MgCc	49E 33 N	312.8	C1C12B	4.67	0.25	0.13	12.10	0.85	31.30	10.35	0.01	0.01	2.59	34.35	96.6	86	4	80	3936	6176	271	393	20	134	20	360	380	116	14	127	6
Catalão I	Magneti-tite	49E 33 N	338.3	C1C13	5.52	1.33	0.05	65.30	0.24	5.83	5.43	0.13	1.22	3.12	9.10	97.3	32	2	421	4780	3237	22	3137	<20	740	30	1270	230	5	3	6	80
Catalão I	MgCc	49E 33 N	357.4	C1C14	0.22	–	0.02	1.37	0.61	46.81	0.92	0.01	0.03	0.09	50.89	101.0	15	1	5	223	2120	19	6	20	12	20	10	70	4	1	8	2
Catalão I	Apatitite	49E 33 N	510.0	C1C22	3.87	1.83	0.14	58.21	0.30	5.27	13.19	0.47	0.84	6.37	5.23	95.5	30	6	522	10620	9279	42	4810	<20	140	30	180	250	17	5	11	51

Site	Rock	Borehole no.	Depth below ground-level	Sample	Nb (ppm)	Mo	Ag	In	Sn	Sb	Cs	La	Ce	Pr	Nd	Sm	Eu	Gd	Tb	Dy	Ho	Er	Tm	Yb	Lu	Hf	Ta	W	Tl	Pb	Bi	Th	U	Th/U
Catalão II	CaCc	C3B2 (A)	79.2	C2A2	109	<2	<0.5	<0.2	<1	1.6	0.6	388	750	81.1	269	32.9	8.74	21.8	2.3	8.9	1.4	3.4	0.41	2	0.25	0.5	0.7	<1	0.1	26	<0.4	7.5	0.8	9.4
Catalão II	Syenite	C3B2 (A)	109.7	C2A6	102	<2	<0.5	<0.2	4	2.5	1.6	144	330	40.5	152	20.6	5.4	13.3	1.3	5.2	0.7	1.7	0.22	1.2	0.16	4	5.7	2	0.2	39	<0.4	10.4	0.5	20.8
Catalão II	Phl-Picrite	C3B2 (A)	137.8	C2A8	317	2	0.5	0.2	9	3.9	2.7	323	674	78.3	230	37.6	9.93	25.5	2.8	10.6	1.5	3.4	0.39	1.9	0.21	20.8	16.9	1	0.3	24	0.4	35.4	7	5.1
Catalão II	Phl-Picrite	C3B2 (A)	161.2	C2A10	251	<2	1.8	<0.2	4	4.5	2.8	307	584	69.1	246	34.2	9.29	23.5	2.6	10.8	1.7	3.9	0.45	2.3	0.26	23.3	14.4	<1	0.4	151	1.3	30	7.6	3.9
Catalão II	Phlogopi-tite	C3B2 (A)	165.2	C2A11	195	<2	2.8	<0.2	<1	7.6	3.2	143	351	45.3	176	26.3	7.01	17.1	1.8	7.1	1	2.3	0.27	1.2	0.13	20.2	8	<1	0.9	63	<0.4	24.5	3.3	7.4
Catalão II	CaCc	C3B2 (A)	271.2	C2A15	15	<2	<0.5	<0.2	<1	3.5	<0.5	656	1040	108	328	44.3	11.6	28	3.3	14.5	2.2	5.4	0.64	3.3	0.4	0.4	0.3	1	0.1	28	<0.4	70.8	2.1	33.7
Catalão II	CaCc	C3B2 (A)	287.0	C2A17	18	2	0.5	0.2	1	3	0.5	366	649	69.4	181	25.6	6.71	17.4	1.7	6.4	0.9	2	0.25	1.3	0.17	0.3	0.3	1	0.2	5	0.4	7.8	0.8	9.8
Catalão II	Phl-Picrite	C3B2 (A)	290.1	C2A18	277	2	0.5	0.2	3	1.3	2.7	308	611	71.4	202	32.7	8.55	22	2	8.2	1.1	2.5	0.28	1.4	0.16	13.6	18.4	1	0.2	16	0.4	35	6	5.8
Catalão II	CaCc	C3B2 (A)	314.0	C2A19	80	5	0.5	0.2	1	0.7	0.5	421	820	91.1	245	35.7	8.96	22.9	2.3	9.1	1.3	2.9	0.32	1.5	0.18	2.4	2.6	1	0.5	16	0.4	10.5	4.2	2.5
Catalão II	CaCc	C3B2 (A)	320.0	C2A20	13	3	0.5	0.2	1	1.5	0.5	482	893	93.6	244	34.3	8.86	22.6	2.3	9.3	1.4	3.3	0.39	1.8	0.22	1.4	0.2	1	0.5	5	0.4	13.4	3.1	4.3
Catalão II	CaCc	C3B2 (A)	324.8	C2A21	90	2	0.5	0.2	1	1.1	0.5	419	824	88.6	217	32.6	8.36	22.7	2	8.1	1.2	2.7	0.32	1.5	0.17	0.8	3.5	1	0.1	5	0.4	7.7	1.5	5.1
Catalão II	Magne-titite	C3B2 (A)	353.1	C2A24	>1000	<2	4.4	0.2	27	2.5	1	310	1550	167	600	84.1	22	42.6	4.2	15.8	2	4.4	<0.05	1.8	0.14	32.5	9.7	8	0.2	130	1	1610	21.5	74.9
Catalão II	Apatitite	C3B1 (B)	127.7	C2B3	197	<2	1.5	<0.2	5	4.2	1	405	1030	131	511	75.5	20	53	5.3	19.4	2.7	6.4	0.75	3.4	0.36	19.3	14.2	5	0.2	89	<0.4	29.5	3.7	8.0
Catalão II	CaCc	C3B1 (B)	308.5	C2B17	14	2	0.5	0.2	1	4	0.5	398	742	76.2	189	27.3	7.13	18.7	1.8	7.2	1	2.5	0.29	1.4	0.16	0.2	0.2	1	0.1	6	0.4	1.4	0.8	1.8
Catalão II	FeCc	C3B1 (B)	312.9	C2B18	238	2	0.5	0.2	1	0.9	1.6	485	1060	123	329	48	11.7	32.8	3.2	13.5	2.2	5.5	0.68	3.5	0.43	0.6	7.5	2	0.1	6	0.4	29.5	30.3	1.0
Catalão II	CaCc	C3B1 (B)	328.5	C2B19	127	2	0.5	0.2	1	0.5	0.5	388	784	85.7	224	32.5	8.22	21.3	2	7.3	1	2.4	0.26	1.2	0.12	1	3.4	1	0.3	5	0.4	4.6	2.9	1.6
Catalão II	CaCc	C3B1 (B)	354.0	C2B22	17	3	<0.5	<0.2	<1	3.4	<0.5	614	1180	136	464	79.7	23	60.5	7.1	29	4.4	9.8	1.08	5.6	0.65	0.6	0.5	<1	<0.1	29	<0.4	96.7	4.4	22.0
Catalão II	Phl-Picrite	C3B1 (B)	368.8	C2B23	278	<2	0.7	<0.2	4	4.1	2.8	272	518	57.9	200	27.1	7.15	18.6	1.9	8	1.2	3	0.36	1.8	0.2	20.6	17.9	<1	0.2	97	1.1	26.8	6.1	4.4
Catalão II	FeCc	C3B1 (B)	400.0	C2B24	40	<2	<0.5	<0.2	<1	2.1	0.5	442	857	91.8	312	38.1	10.1	24.8	2.4	9.5	1.4	3.2	0.37	1.9	0.2	10.3	2.1	<1	0.2	9	<0.4	5.4	0.8	6.8
Catalão I	Magne-titite	F72	100.0	C1A5	>1000	<2	1.5	0.5	59	<0.5	<0.5	120	317	41.7	143	19	4.72	10.7	1	3.8	0.5	1.1	<0.05	0.6	0.05	37.1	277	<1	<0.1	12	<0.4	380	735	0.5
Catalão I	MgCc	3E 19 N	175.0	C1B10	213	2	0.5	0.7	14	0.5	0.5	2000	3000	1000	2000	359	84.6	209	17.7	56.4	7	16.5	<0.05	4.9	0.2	9	0.1	1	0.3	50	0.4	21.2	11.6	1.8

Table 1 continued

Site	Rock	Borehole no.	Depth below ground-level	Sample	Nb (ppm)	Mo	Ag	In	Sn	Sb	Cs	La	Ce	Pr	Nd	Sm	Eu	Gd	Tb	Dy	Ho	Er	Tm	Yb	Lu	Hf	Ta	W	Tl	Pb	Bi	Th	U	Th/U
Catalão I	MgCc	49E 33 N	114.8	C1C2	53	2	0.5	0.2	5	4.4	0.5	2000	3000	1000	2000	533	112	260	18.2	52.6	6.3	16.7	<0.05	1.2	0.04	1.1	0.1	1	3.8	112	1.3	19	7.9	2.4
Catalão I	MgCc	49E 33 N	130.0	C1C4	231	2	0.5	0.2	2	3.2	0.5	729	1660	189	569	86.3	23.1	53.8	4.6	14.4	1.6	2.6	<0.05	0.7	0.04	0.9	0.1	1	0.1	7	0.4	26	5.4	4.8
Catalão I	MgCc	49E 33 N	312.8	C1C12B	434	2	0.5	1.1	10	0.5	0.5	2000	3000	1000	2000	537	121	277	24.3	76.7	9.8	22.7	<0.05	5.2	0.05	10.5	6.9	1	11.1	37	0.4	44.8	96.9	0.5
Catalão I	Magne-titite	49E 33 N	338.3	C1C13	>10000	30	7.3	<0.2	16	1.3	0.5	365	884	105	371	45.2	11.1	27.8	2.5	8.3	1.1	2.5	<0.05	1	0.09	79.5	56.3	1	9.2	30	<0.4	192	640	0.3
Catalão I	MgCc	49E 33 N	357.4	C1C14	9	2	0.5	0.2	1	0.8	0.5	326	727	85.4	273	46.8	11.5	26.2	2.3	7	0.8	1.5	<0.05	0.5	0.04	0.4	0.1	1	0.1	5	0.4	3.2	0.4	8.0
Catalão I	Apatitite	49E 33 N	510.0	C1C22	>1000	<2	10.2	<0.2	21	<0.5	<0.5	1390	>3000	367	1240	142	34	81.1	6.5	18.7	2.6	5.5	<0.05	1.6	0.1	96	55.5	<1	1.2	162	1	990	495	2.0

Phl-Picrite phlogopite-picrite (Guarino et al. 2013); *CaCc* calciocarbonatite; *FeCc* ferrocarbonatite; *MgCc* magnesiocarbonatite

(baddeleyite), Sr–Nd–Hf isotopic and trace elemental analyses of minerals (baddeleyite and pyrochlore) have been performed at the Institute of Geology and Geophysics, Chinese Academy of Sciences, Beijing (China). Major element compositions were obtained using a JEOL–JAX8100 electron microprobe with 15 kV accelerating potential and 12 nA beam current. Trace element compositions (including REE) and U–Pb isotopic compositions of baddeleyite and pyrochlore were performed by using an Agilent 7500a LA–ICP–MS instrument, with the full analytical details described in Xie et al. (2008). The in situ Sr–Nd analyses of pyrochlore were carried out using a Neptune MC–ICP–MS. The detailed description of the instrument and laser ablation system is found in Yang et al. (2009). Hf isotopic composition of baddeleyite was obtained by MC-ICP-MS instrument.

Full analytical details are reported in the "Analytical Techniques" as Supplementary File.

Classification and petrography

Modal and chemical data have been used to classify the Catalão II rocks (Table 1; Supplementary Table 1). The rocks of Catalão II are carbonatites, magnetite-, apatite- and phlogopite-rich rocks, lamprophyres and associated fenitized rocks.

The carbonatites are calciocarbonatites and ferrocarbonatites (Fig. 3; Woolley and Kempe 1989). The ferrocarbonatites may have high modal phlogopite (17–27 vol.%). The magnetite- and apatite-rich rocks following modal classification are classified as magnetitites and phlogopite–magnetite apatitites. For simplicity, the latter will be referred to as apatitites in the text. The phlogopite-rich rocks are described as phlogopitites or glimmerites. The lamprophyres are phlogopite-rich, SiO_2-poor (SiO_2 = 29.3–31.7 wt%), MgO-rich (MgO = 14.4–18.7 wt%), TiO_2-rich (4.6–6.5 wt%), Al_2O_3-poor (3.9–4.7 wt%) and ultrapotassic (K_2O/Na_2O = 12.6–32). Their mineralogical and bulk-rock composition, and their association with carbonatites, allowed us to classify them as ultramafic lamprophyres (IUGS classification; Tappe et al. 2005). For clarity, following Gibson et al. (1995), Brod et al. (2000) and Guarino et al. (2013), we still continue to refer them to as phlogopite-picrites. The associated fenitized rocks in Catalão II are syenites and clinopyroxenites (see below). All lithologies are inequigranular holocrystalline, with cumulitic texture, with the exception of the phlogopite-picrites with a porphyritic texture and clinopyroxenite with a banded structure.

At Catalão II, the C3B2(A) borehole intersects calciocarbonatites, phlogopite-picrites, phlogopitites, magnetitites, apatitites and fenites, and the C3B1(B) borehole

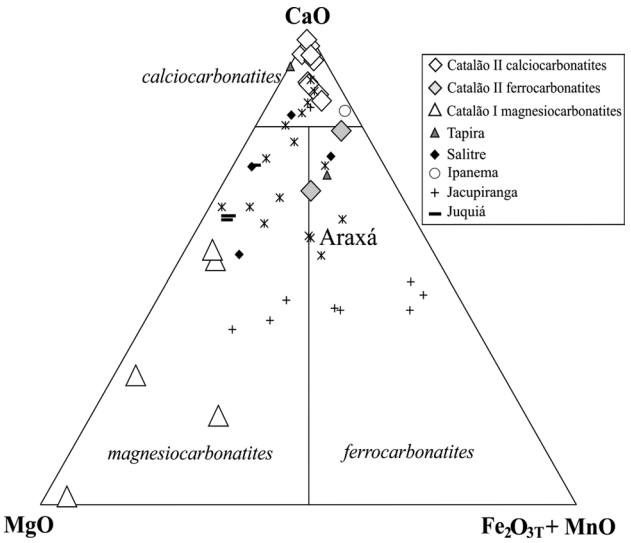

Fig. 3 Chemical classification of the Catalão II and Catalão I carbonatites (Woolley and Kempe 1989). The Araxá (Traversa et al. 2001), Tapira (Gomes and Comin-Chiaramonti 2005), Salitre (Morbidelli et al. 1997), Ipanema (Guarino et al. 2012), Jacupiranga (Huang et al. 1995) and Juquiá (Beccaluva et al. 1992) carbonatites are also shown

intersects calciocarbonatites, ferrocarbonatites, phlogopitite, apatitites and phlogopite-picrites. The most representative lithotypes are reported in Fig. 4.

The Catalão I carbonatites are magnesiocarbonatites (Fig. 3), while the magnetite- and apatite-rich rocks, following modal classification, are simply named as magnetitite and apatitite, although these rocks show variable modal contents in phlogopite, apatite/magnetite and carbonate (Supplementary Table 1). At Catalão I, the F72 borehole intersects magnetitites; the 3E19 N borehole intersects magnesiocarbonatites, and the 49E33 N borehole cuts magnesiocarbonatites, magnetitites and apatitites.

Catalão II complex

The *calciocarbonatites* and *ferrocarbonatites* are characterized by medium- to coarse-grained anhedral carbonates, and minor amounts of macro- and microcrysts of zoned phlogopite, slightly orange in the core and dark orange in the rims, apatite, magnetite, pyrochlore, carbonates, rutile, rare clinopyroxene and amphibole. The *magnetitites* are characterized by medium- to coarse-grained magnetite associated with subordinate phlogopite, apatite, pyrochlore and carbonates. The *apatitites* are medium- to coarse-grained rocks and consist of apatite and phlogopite, with minor opaques, carbonates and pyrochlore. The *phlogopitites* have phlogopite as the dominant phase and contain minor magnetite, pyrochlore and apatite, and rare accessory carbonates. The C2B5 phlogopitite is cross-cut by a calciocarbonatite showing embayed zircon crystals with corroded and altered rims. The *phlogopite-picrites* have a porphyritic texture with olivine and phlogopite phenocrysts in a pseudo-fluidal groundmass rich in phlogopite laths and made up also of olivine, spinel, apatite, perovskite, calcite and rare garnet and rutile. *Syenites and amphibole clinopyroxenites (fenitized rocks).* The syenite C2A6 is dominated by alkali feldspar, with minor Na-rich clinopyroxene, phlogopite, amphibole and apatite. The clinopyroxenite C2A26 has a banded structure; the alternating bands are formed by Na-rich clinopyroxene and amphibole and by minor phlogopite. Apatite and carbonate are accessory phases and iron oxides are absent. The syenites and amphibole clinopyroxenites are *fenites*, i.e. the products of interaction of Na- and K-rich fluids, likely coming/derived from the carbonatite intrusion, with the host rocks (Le Bas 2008; Guarino et al. 2012).

Catalão I complex

Two types of *magnesiocarbonatites* are found in the Catalão I complex. The first one is made up of cryptocrystalline carbonate and the second type by medium- to coarse-grained anhedral carbonate crystals associated with minor phlogopite, apatite, carbonates, zoned pyrochlore and rare monazite. *Magnetitites* and *apatitites* consist of anhedral magnetite and/or apatite as dominant phases, with minor phlogopite, carbonate, pyrochlore and rare baddeleyite. A few olivine phenocrysts, commonly altered, were also observed.

Mineral chemistry

Mineral analyses of Catalão II and Catalão I rocks are reported in the Supplementary Tables 2 to 12.

Carbonates. Calcite ($CaCO_3$) is the dominant phase of calciocarbonatites and ferrocarbonatites at Catalão II, with minor dolomite [$CaMg(CO_3)_2$], strontianite ($SrCO_3$), alstonite [$BaCa(CO_3)_2$], ankerite [$Ca(Fe^{2+},Mg,Mn^{2+})(CO_3)_2$], siderite ($Fe^{2+}CO_3$), Mg-rich siderite [$(Fe^{2+},Mg)CO_3$], burbankite [$(Na,Ca)_3(Sr,Ba,Ce)_3(CO_3)_5$], olekminskite [$(Sr,Ca,Ba)_2(CO_3)_2$], shortite [$Na_2Ca_2(CO_3)_3$] and ancylite-Ce [$Sr(Ce,La)(CO_3)_2(OH)(H_2O)$]. Ankerite is found in apatitite; calcite is found in magnetitite, phlogopite-picrites and phlogopitite; calcite and alstonite are found in the fenites (Supplementary Table 2). The chemical compositions of carbonates are reported in Fig. 5. Similar carbonates were analysed in the Catalão I magnesiocarbonatites, with predominant dolomite followed by calcite, ferroan magnesite [$(Mg,Fe^{2+})CO_3$], magnesite ($MgCO_3$), strontianite, witherite ($BaCO_3$), alstonite, norsethite [$BaMg(CO_3)_2$], burbankite and olekminskite (Supplementary Table 2). Dolomite, norsethite, calcite and burbankite are present in magnetitites, whereas dolomite and calcite are

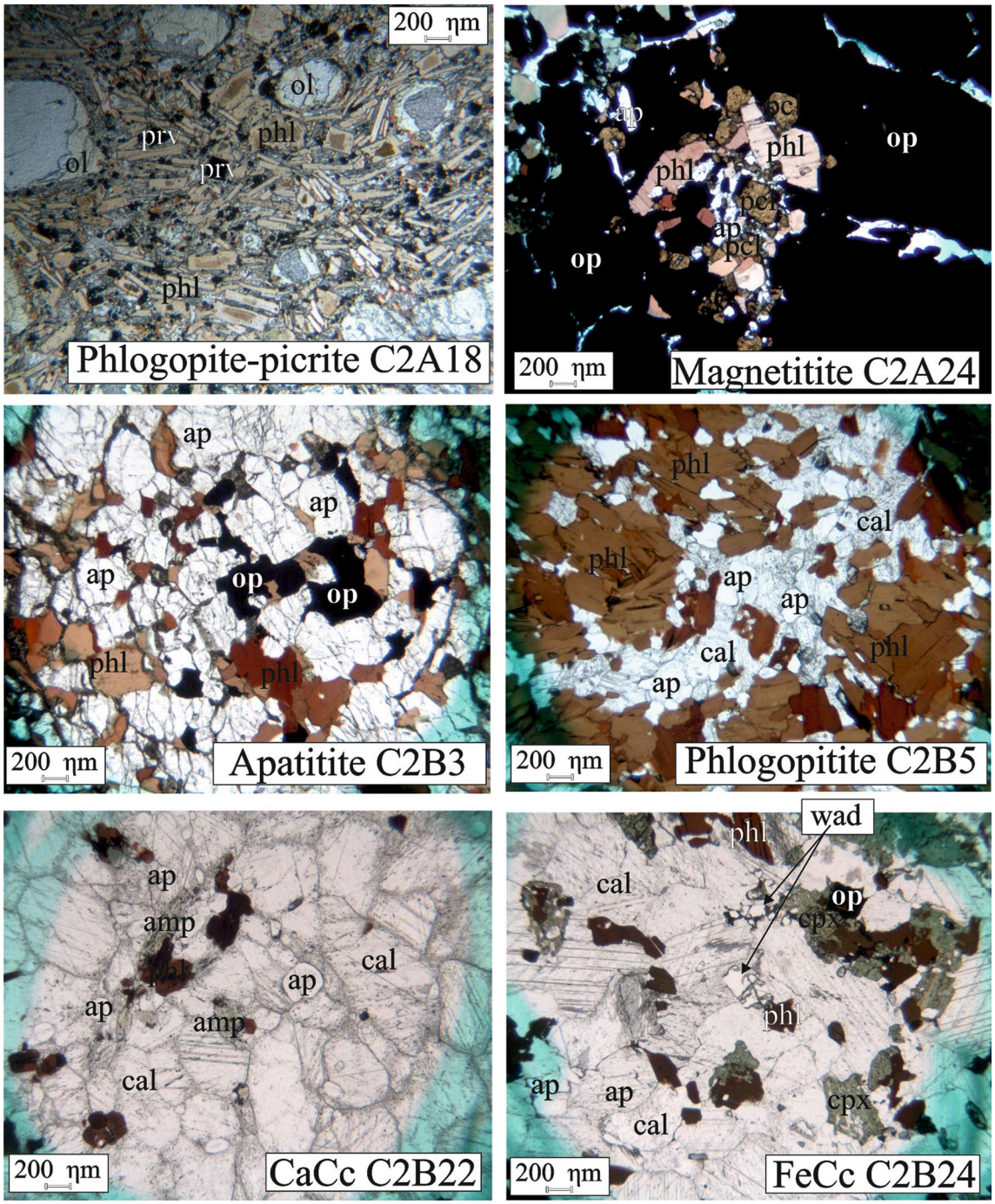

Fig. 4 Representative thin-section photomicrographs of Catalão II rocks. *CaCc* calciocarbonatite; *FeCc* ferrocarbonatite; *amp* amphibole; *ap* apatite; *cal* calcite; *cpx* clinopyroxene; *op* opaque mineral; *pcl* pyrochlore; *phl* phlogopite; *prv* perovskite; and *wad* wadeite

common in apatitites. Burbankite, ancylite and norsethite have also been found in other carbonatites of the APIP, for example, at Araxá (cf. Traversa et al. 2001).

Mica is an essential phase of the Catalão II rocks and belongs to the phlogopite-tetra-ferriphlogopite series (Supplementary Fig. 1a), as is evident from the presence of Fe^{3+} in the tetrahedral site (i.e. $Si^{4+}+{}^{IV}Al^{3+}$ <4) (M.F. Brigatti and V. Guarino *work in progress*).

The phlogopite-picrites, ferrocarbonatites and phlogopitites of Catalão II contain phlogopite and tetra-ferriphlogopite. Mica of ferrocarbonatites and phlogopitites has different ranges in Mg# [as Mg/(Mg + Fe^{2+})], 0.39–0.65

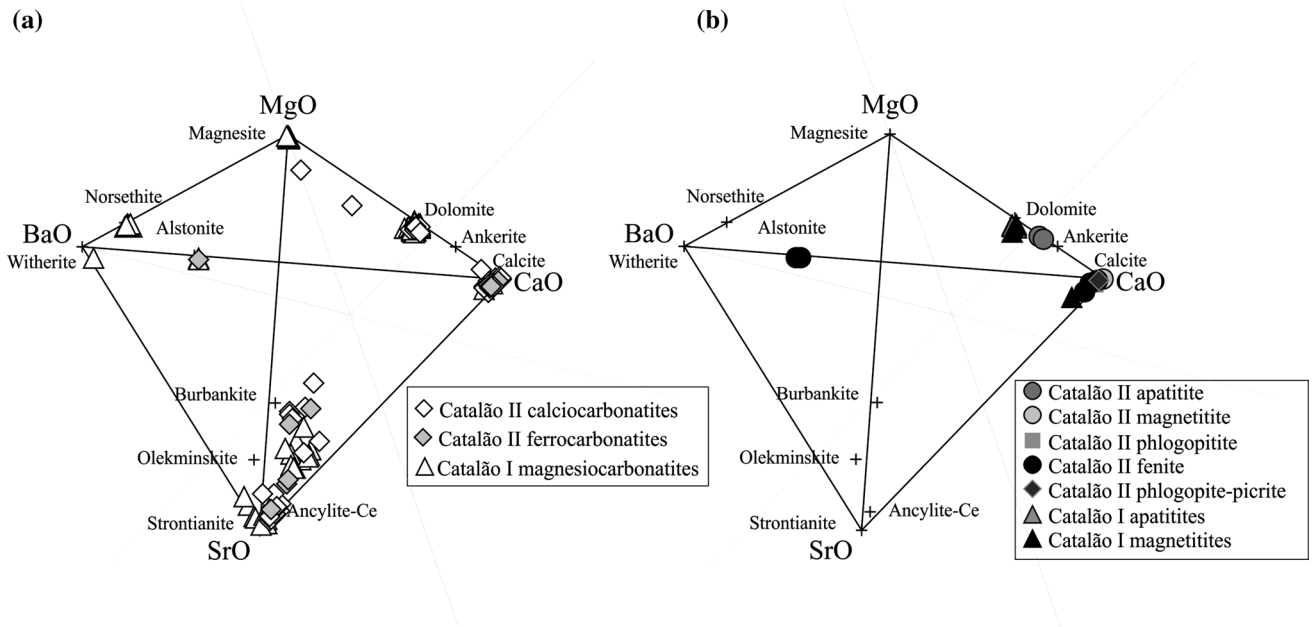

Fig. 5 Proposed classification diagram for the carbonate minerals (in wt%) in the Catalão II and Catalão I carbonatites (**a**) and other rock types (**b**). The tetrahedral diagram has been made using the Tetra-Plot spreadsheet (Cucciniello 2016). The dolomite, calcite, magnesite, ankerite, norsethite, alstonite, witherite, strontianite, ancylite-Ce, olekminskite and burbankite compositions (+) are taken from the Handbook of Mineralogy

and 0.63–0.77, respectively. The TiO_2 concentration ranges between 0.17 and 1.20 wt% in phlogopitites and between 0.15 and 2.39 wt% in ferrocarbonatites. Mica of phlogopite-picrites has the highest variability in Mg# (0.16–0.87) and TiO_2 (0.44–4.91 wt%). Tetra-ferri-phlogopite is present in Catalão II apatitite, magnetitites and calciocarbonatites, with similar Mg# (0.52–0.71) and TiO_2 (up to 0.75 wt%). The Catalão II fenites have phlogopite/biotite (Mg# = 0.54–0.68, TiO_2 = 0.74–1.20 wt%).

Fe–Ti oxides. The chemical compositions of Fe–Ti oxides investigated in this study are shown in Supplementary Fig. 1b. *Magnetite* is ubiquitous in the Catalão II rocks, and it is absent in the fenites. Magnetite and Ti-magnetite (Supplementary Table 3) are found in apatitites, magnetitites, phlogopitites and calciocarbonatites of Catalão II and in magnesiocarbonatites, apatitites and magnetitites of Catalão I. Their compositions have a wide range in ulvöspinel (0–29 mol% ulvöspinel). The Catalão II phlogopite-picrites have Ti-magnetite (8–30 mol% ulvöspinel, 4.1–17.4 wt% TiO_2), magnesiochromite [Cr# as Cr/(Cr + Al) = 0.86–0.87; Mg# = 0.52–0.58] and chromite [Cr# = 0.85; Mg# = 0.45].

Ilmenite of the Catalão II calciocarbonatites has 88–93 mol% ilmenite, similar to the composition of this phase in the Catalão I apatitites and magnetitites (89–95 mol% ilmenite; Supplementary Table 3). Ilmenite from the two complexes contains variable concentration of MgO (0.7–7.4 wt% in Catalão I apatitites and magnetitites and 1.1–3.7 wt% in Catalão II calciocarbonatites) and plots mainly in the field of non-kimberlitic ilmenites (Supplementary Fig. 1c; Wyatt et al. 2004). Equilibrium temperatures and oxygen fugacity of one pair of coexisting magnetite and ilmenite from Catalão I apatitites give 878 °C, and 10^{-12} bars fO_2, and plot along the NiNiO buffer (Supplementary Fig. 1d).

Rutile. Tiny crystals of *rutile* (TiO_2) have been found in Catalão II calciocarbonatites and phlogopite-picrites (Supplementary Fig. 1b; Supplementary Table 3).

Apatite is ubiquitous (Supplementary Table 4). In the Catalão II complex, the SrO concentration of apatite in magnetitite, phlogopitite and apatitite is <1.4 wt% and ranges from 1.1–2.1 wt% in apatite of the calciocarbonatites. The fluorine concentration is quite similar in the Catalão II rocks (~3.7 wt% in apatitite, 3.1 wt% in magnetitite, 3.5–3.8 wt% in phlogopitite and 3.5–3.8 wt% in calciocarbonatite). In the Catalão I complex, the concentration of SrO (up to 7.1 wt%) and F (up to 3.6 wt%; data of this work and Cordeiro et al. 2010) in apatite of magnesiocarbonatites is different to those in apatite of apatitites and magnetitites (SrO up to 4.7 wt%; *F* up to 3.3 wt%).

Pyrochlore is a ubiquitous phase of Catalão II magnetitites and ferrocarbonatite, and of Catalão I apatitites, magnetitites and magnesiocarbonatites (Supplementary Table 5). Pyrochlore shows marked zoning and a bimodal

chemical composition: the first pyrochlore is characterized by Ca > 0.8 apfu, Na > 0.45 apfu, Ba < 0.1 apfu, Ca + Na > 1.25 apfu and F > 0.4 apfu (Fig. 6) and is dark grey in BSE images (Fig. 7); the second is light grey in BSE images (Fig. 7) and has Ca < 0.8 apfu, Na < 0.45 apfu, Ba > 0.1 apfu, Ca + Na < 1.25 apfu and F < 0.4 apfu (Fig. 6). The pyrochlore crystals in Catalão II ferrocarbonatite (C2B18) and in Catalão I (C1A5) have complex zoning pattern reflecting complex chemical patterns of Ca–Na–F-rich (dark grey in BSE) and Th–U–rich (light grey in BSE) compositions (Fig. 7). In the Catalão I C1A5, magnetitite pyrochlore has Ca–Na–F-rich cores and Th–U-rich rims, whereas in the Catalão I C1C20 magnetitite, it has Th–U-rich cores and a Ca–Na–F-rich rims (Fig. 7). The Catalão II pyrochlores are similar to those analysed in Catalão I rocks (this work and Cordeiro et al. 2010, 2011b) and at Sokli, Finland (Lee et al. 2006) (Fig. 6).

The Catalão I pyrochlore is strongly enriched in light REE (La + Ce + Nd ~10,000 ppm) and has highly fractionated REE patterns, with La up to ~11,000–22,000 times chondrite, and high LREE/HREE ratios (La_N/Yb_N = 629–843 in magnetitites and 1411 in apatitite; Supplementary Fig. 2; Supplementary Table 6).

Minor phases at Catalão II. Olivine is found as phenocrysts in phlogopite-picrites with $Fo_{88–89}$ composition [Fo = Mg × 100/(Mg + Fe)] (Supplementary Table 7). *Perovskite* has been found in the phlogopite-picrites. It has dominant $CaTiO_3$ molecule (88–97 mol%; Supplementary Table 8) and is strongly enriched in light REE (~6900–7800 ppm) with La up to ~20,000 times chondrite and high LREE/HREE ratios (La_N/Yb_N ~770–870; Supplementary Fig. 2; Supplementary Table 6). The composition of the Catalão II perovskite matches that found in other APIP rocks and elsewhere (Melluso et al. 2008, 2010; Guarino et al. 2013). *Garnet* is a groundmass phase of the phlogopite-picrites (Supplementary Table 9). The compositions are solid solutions of andradite ($Ca_3Fe_2Si_3O_{12}$; 8–59 mol%) and morimotoite ($Ca_3TiFe^{2+}Si_3O_{12}$; 8–70 mol%) (according to the classification of Locock 2008). Tiny crystals of *wadeite* ($K_2ZrSi_3O_9$) have been found in the C2B24 ferrocarbonatite. *Zircon* ($ZrSiO_4$) has been found in a small vein of calciocarbonatite cutting the C2B5 phlogopitite (Fig. 7). *Clinopyroxene* is aegirine-augite in the fenites and in C2B24 ferrocarbonatite [Mg# = 71–80 and $Na_{17–46}Mg_{40–59}Fe^{2+}_{14–24}$ for fenites, and Mg# 45–66 and $Na_{24–77}Mg_{11–49}Fe^{2+}_{12–27}$ for C2B24 ferrocarbonatite] (Supplementary Table 10). *Amphibole* is K-richterite in the C2A6 fenite and C2B22 calciocarbonatite (Supplementary Table 11; following Leake et al. 1997; Locock 2014). *Barite* ($BaSO_4$) has been found in some calciocarbonatites and ferrocarbonatites. *Alkali feldspar* is found in the C2A6 fenite. It is pure orthoclase ($Or_{99–97}Ab_{0–2}An_{0–1}$; Supplementary Table 12).

Minor phases at Catalão I. Baddeleyite (ZrO_2) was found in magnetitites and apatitite (Supplementary Figs. 2 and 3; Supplementary Table 6) and shows a marked LREE enrichment (La_N ~2000–3000 times chondrite) and LREE/HREE fractionation (La_N/Yb_N = 26–33 in magnetitites and La_N/Yb_N = 13 in apatitites; Supplementary Fig. 2). Baddeleyite has a different trace element pattern compared to pyrochlore and perovskite, as a response to its completely different crystal chemistry. *Olivine* is an accessory phase in magnetitites and has a high forsterite content ($Fo_{97–98}$; Supplementary Table 7). This very high forsterite content is far outside the range found in mantle-derived silicatic rocks, kimberlites or mantle lithologies; rather, it is fairly common in carbonatites (Araxá; Traversa et al. 2001; Salitre; Morbidelli et al. 1997; Sung Valley, India; Melluso et al. 2010) and in skarns formed from dolomitic lithologies (e.g. Wenzel et al. 2002). *Monazite* [(La, Ce, Nd)PO_4] and *pyrite* (FeS_2) were found in magnesiocarbonatites (Supplementary Table 4).

Geochemistry

Major elements

The phlogopite-picrites (n = 4) are ultrabasic (SiO_2 = 29.3–31.7 wt%), ultrapotassic (K_2O = 3.3–4.6 wt% and K_2O/Na_2O = 13–32), ultramafic (MgO 14.4–18.7 wt%) and moderately CaO-rich (8–11.2 wt%) rocks; they represent primitive magmatic compositions, as are the APIP kamafugites/kimberlites cropping out all around Catalão II (Gibson et al. 1995; Brod et al. 2000; Araújo et al. 2001; Melluso et al. 2008; Guarino et al. 2013). The calciocarbonatites (n = 9) have low Fe_2O_{3t} (0.4–5.2 wt%), SiO_2 (0.3–4.3 wt%) and MgO (0.6–2.8 wt%) with limited CaO variability (from 46 to 53.6 wt%). The ferrocarbonatites (n = 2) have moderate Fe_2O_{3t} (8.4–8.9 wt%), SiO_2 (8.8–14.9 wt%) and MgO (2.3–8.1 wt%) at CaO from 33 to 43.1 wt%. The apatitite and magnetitite (n = 2) have high and variable Fe_2O_{3t} (32–63.3 wt%) and CaO (4.6–24.1 wt%), with low SiO_2 (6.8–10.9 wt%) and MgO (6.6–6.8 wt%). The P_2O_5 in apatitite is 16.7 wt%. The phlogopitite (n = 1) has 30 wt% SiO_2, 15.8 wt% Fe_2O_{3t}, 17.7 wt% MgO and 11.2 wt% CaO. The syenite fenite (n = 1) is potassic (K_2O/Na_2O = 2.5) and has relatively high SiO_2 (44.7 wt%), Fe_2O_{3t} (10.4 wt%), MgO (14.2 wt%) and CaO (10 wt%). The Catalão II rocks show chemical variations, similar to those of the Catalão I rocks (Supplementary Fig. 4).

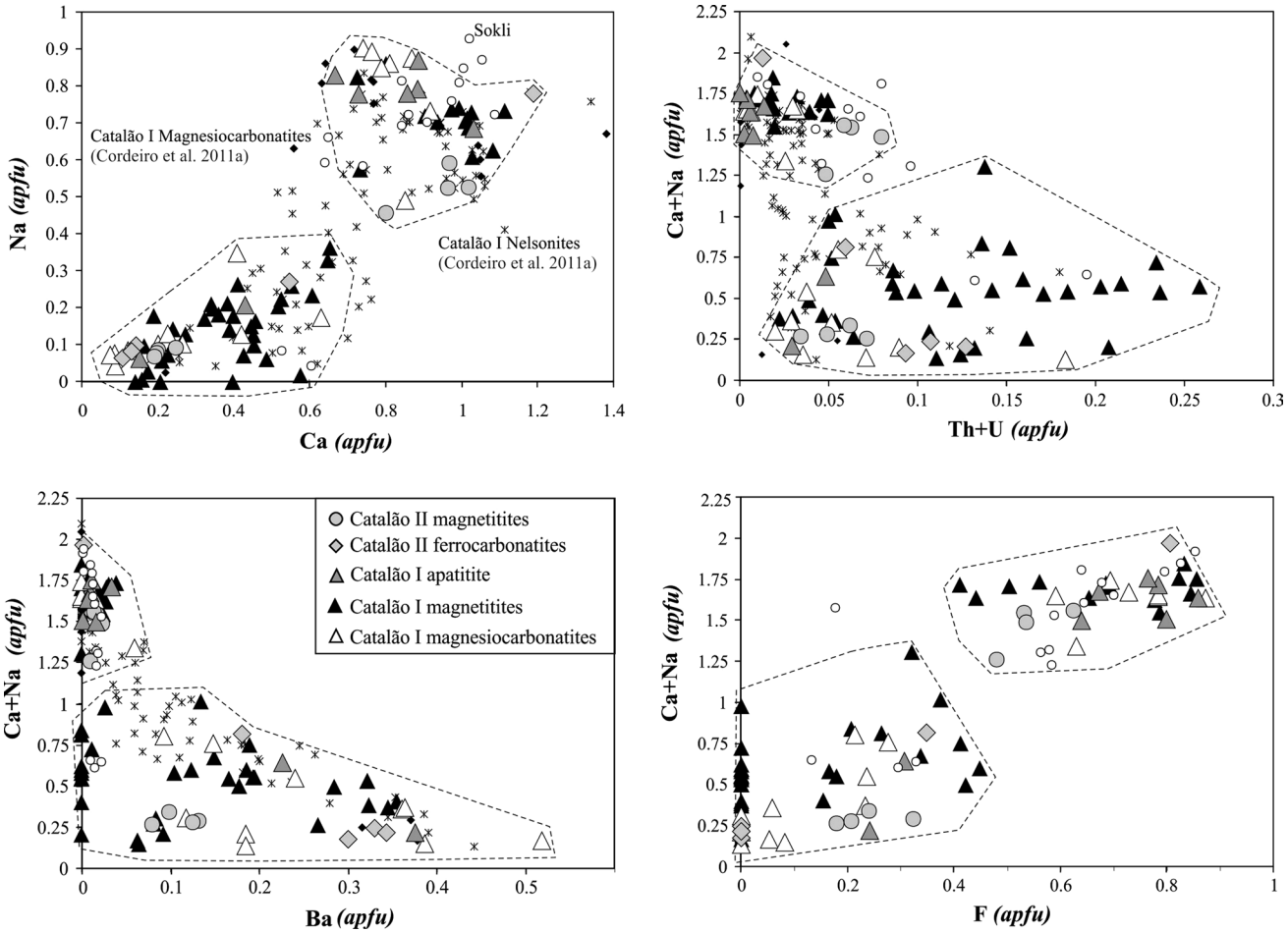

Fig. 6 Representative compositional (apfu) diagrams for pyrochlores from different Catalão II and Catalão I rocks. The chemical compositions of pyrochlores from nelsonites and magnesiocarbonatites from Catalão I are shown for comparison (data from Cordeiro et al. 2010, 2011b). Pyrochlores from the Sokli carbonatites, Finland, are also shown (data from Lee et al. 2006)

REE and other trace elements

The Catalão II phlogopite-picrites have high and variable Cr (270–1040 ppm) and Ni (160–360 ppm) concentrations (Table 1), indicating their primitive nature. The Catalão II magnetitite, apatitite and carbonatites, like those of Catalão I, contain generally low concentration of Cr (<20 ppm) and Ni (<50 ppm). The Catalão II phlogopitite has 130 ppm Cr and 60 ppm Ni. The Catalão II rocks, with those of Catalão I, exhibit highly fractionated REE patterns (La_N/Yb_N up to 218 in Catalão II calciocarbonatites and $La_N/Yb_N = 1124$ in Catalão I magnesiocarbonatites) with $La_N = 400$–2000 times chondrite in Catalão II rocks and 400–7000 times chondrite in Catalão I rocks (Supplementary Fig. 5). Primitive mantle-normalized multielement patterns of the Catalão II phlogopite-picrites and of the Catalão I lamprophyre (Gomes and Comin-Chiaramonti 2005) are generally comparable (Fig. 8b, d). The Catalão II magnetitite is relatively enriched in Th, U and Nb when compared to Catalão II apatitite that show also a trough at Ti. This likely reflects different modal abundances of pyrochlore (Fig. 8c). The Catalão II calciocarbonatites and ferrocarbonatite (C2B18) and some Catalão I magnesiocarbonatites have troughs at K, Ti, Hf and Zr, and a peak at Ba. Some Catalão I magnesiocarbonatites (as in the sample C1C14 and Cordeiro et al. 2010) and Catalão II C2B24 ferrocarbonatite have less evident or no troughs at Zr and Hf (Fig. 8b, d).

Radiogenic and stable isotopes

Nd–Sr isotope composition

New $^{87}Sr/^{86}Sr$ and $^{143}Nd/^{144}Nd$ isotopic data were obtained from Catalão II and Catalão I bulk-rock samples and from perovskite and pyrochlore separates. The results are shown in Table 2 and Fig. 9.

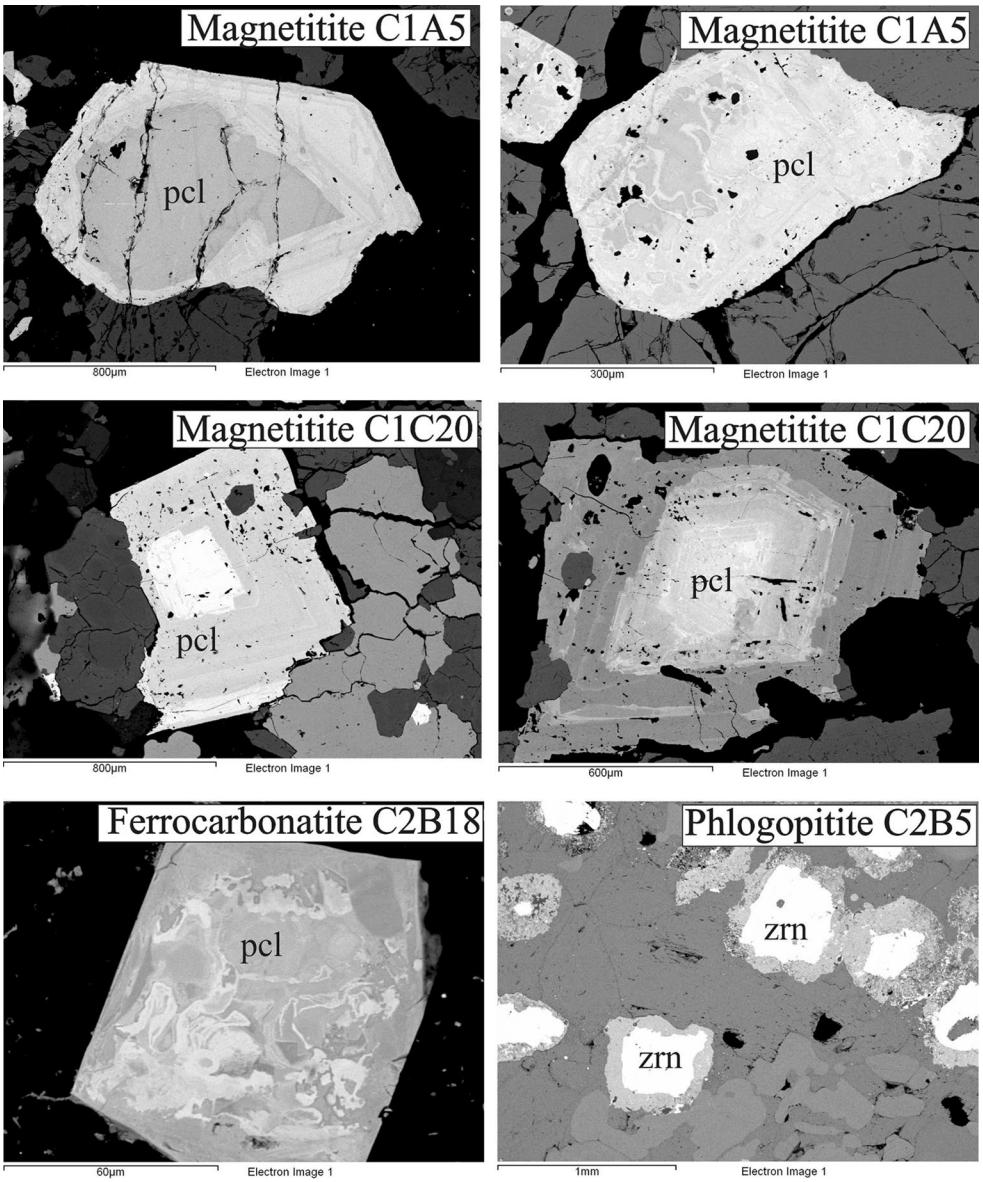

Fig. 7 Representative backscatter electron images (BSE) of pyrochlores (pcl) from different Catalão I and Catalão II rocks (Catalão I C1A5 and C1C20 magnetitites; Catalão II C2B18 ferrocarbonatite). *Dark* and *light* areas correspond to the first and second type of pyrochlore, respectively. The Catalão II C2B5 *phlogopitite* shows the presence of a thin carbonatite vein in which light crystals of zircons (zrn) are included

Catalão II complex

The initial (at 82 Ma) $^{87}Sr/^{86}Sr$ (0.70503–0.70536) and εNd (−6.8 to −4.7) of the calciocarbonatites have restricted variation. The ferrocarbonatites have $^{87}Sr/^{86}Sr_i$ (0.70512–0.70523) and εNd_i (−5.4 to −5.2) overlapping the values of the calciocarbonatites. The phlogopite-picrites have slightly higher $^{87}Sr/^{86}Sr_i$ (0.70531–0.70599) and similar εNd_i (−6.7 to −5.4) values of calciocarbonatites. The syenite fenite has $^{87}Sr/^{86}Sr_i$ of 0.70553 and εNd_i of −6. The T_{DM} Nd model age of the calcio- and ferrocarbonatites varies between 0.7 and 0.9 Ga, similar to variation observed in phlogopite-picrites (0.8–0.9 Ga).

Catalão I complex

The $^{87}Sr/^{86}Sr_i$ of magnetitites and apatitites ranges between 0.70513 and 0.70561, and initial εNd_i (at 81 Ma) between

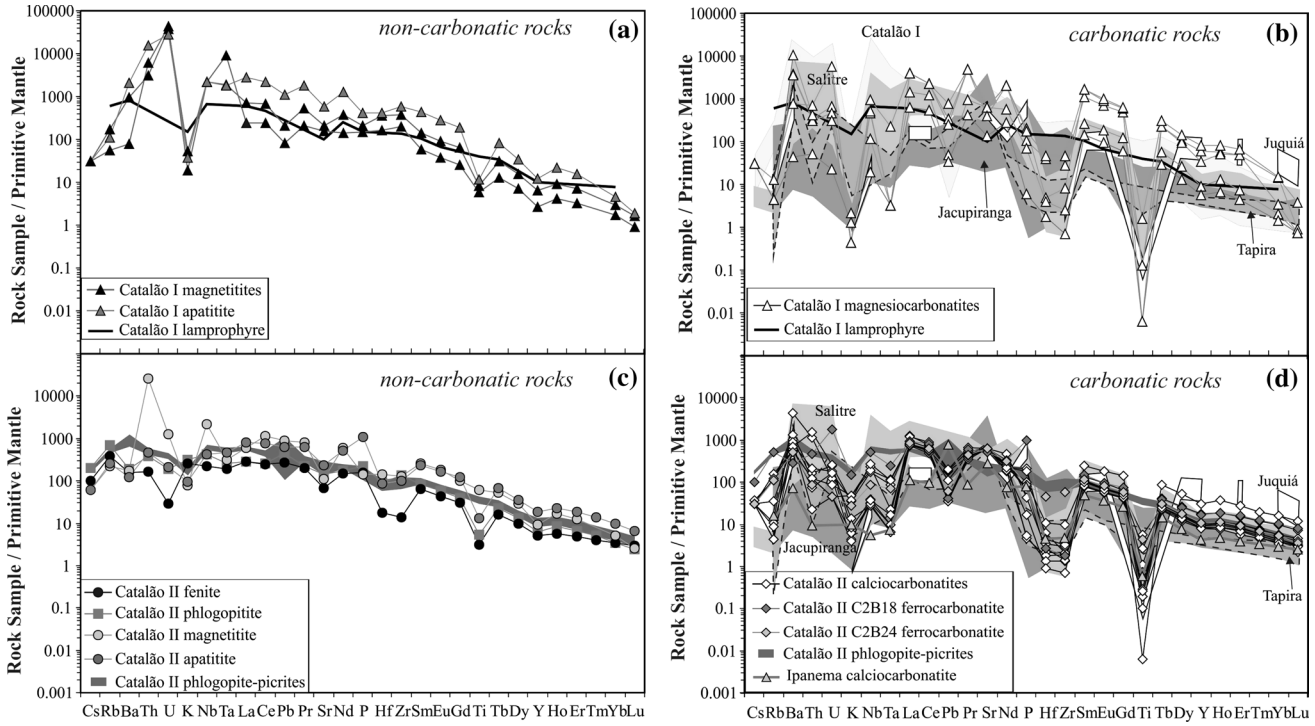

Fig. 8 Primitive mantle-normalized element patterns for Catalão II and Catalão I rocks (normalization values after Lyubetskaya and Korenaga 2007). The chemical compositions of Catalão I lamprophyre (Gomes and Comin-Chiaramonti 2005) and magnesiocarbonatite field (Cordeiro et al. 2010), Catalão II phlogopite-picrite field (Guarino et al. 2013), Tapira (Gomes and Comin-Chiaramonti 2005), Salitre (Morbidelli et al. 1997), Jacupiranga (Huang et al. 1995), Juquiá (Beccaluva et al. 1992) and Ipanema (Guarino et al. 2012) carbonatites are plotted for comparison

−8.1 and −6.9. Pyrochlore separates have $^{87}Sr/^{86}Sr_i$ (0.70531–0.7055) and εNd_i (−7.6 to −6.9) within the range of magnetitites and apatitites. The isotopic composition of magnesiocarbonatites ($^{87}Sr/^{86}Sr_i$ = 0.70529–0.70542; εNd_i = −9.6 to −7.7) is similar to range of magnetitite and apatitite. The T_{DM} Nd model age of the magnesiocarbonatites ranges between 0.9 and 1.9 Ga, higher than that of magnetitites (~0.8 Ga) and apatitites (~0.8 Ga).

The Catalão II and Catalão I rocks plot within the field of APIP kimberlites and kamafugites in the εNd_i vs. $^{87}Sr/^{86}Sr_i$ diagram (Fig. 9). The isotopic composition of Catalão I lamprophyre reported by Gomes and Comin-Chiaramonti (2005) plots within the Catalão II phlogopite-picrite field. The distribution of Nd isotope data in the diagram εNd vs. time (Fig. 10) highlighted as the Catalão II field shows a more limited variation from that of Catalão I.

Hf isotope composition

The hafnium isotopic composition of baddeleyites in Catalão I magnetitites and apatitite is reported in Table 2, Fig. 11 and Supplementary Fig. 6. Baddeleyite is a phase that usually crystallizes in magmas having low silica activity, such as kimberlites and alkaline rocks (cf. also Melluso et al. 2012); differently from zircon, it cannot be considered as a typical mineral that hosts Hf in crustal lithologies; therefore, it can be considered a proxy of the initial Hf isotopic ratio of mantle-derived magmas (cf. Wu et al. 2006). The analysed baddeleyites show a narrow range of initial $^{176}Hf/^{177}Hf$ (0.28248–0.28249) and εHf_i (−10.3 to −10.9). In the εHf_i versus εNd_i diagram (Fig. 11a), the data fall near the field estimated for Group II kimberlites of southern Africa (Nowell et al. 2004 and references therein). The Goiás peridotite xenoliths hosted by kamafugites (Carlson et al. 2007) have distinct εHf_i (Fig. 11a).

The hafnium model ages (T_{DM} Hf) range between 1.0 and 1.1 Ga (Fig. 11b) that broadly corresponds to tectonomagmatic events in the basement, such as the Neoproterozoic Goiás Magmatic Arc, of central southern Brazil (cf. Matteini et al. 2010 and reference therein).

C–O isotope composition

The C–O isotope compositions are reported in Table 3. In the Catalão II complex, calcite of calciocarbonatites has $\delta^{18}O$ = 8.46–9.36 ‰ ($\delta^{13}C$ = −6.35 to −5.68 ‰), and calcite in ferrocarbonatites has $\delta^{18}O$ = 8.45–9.48 ‰

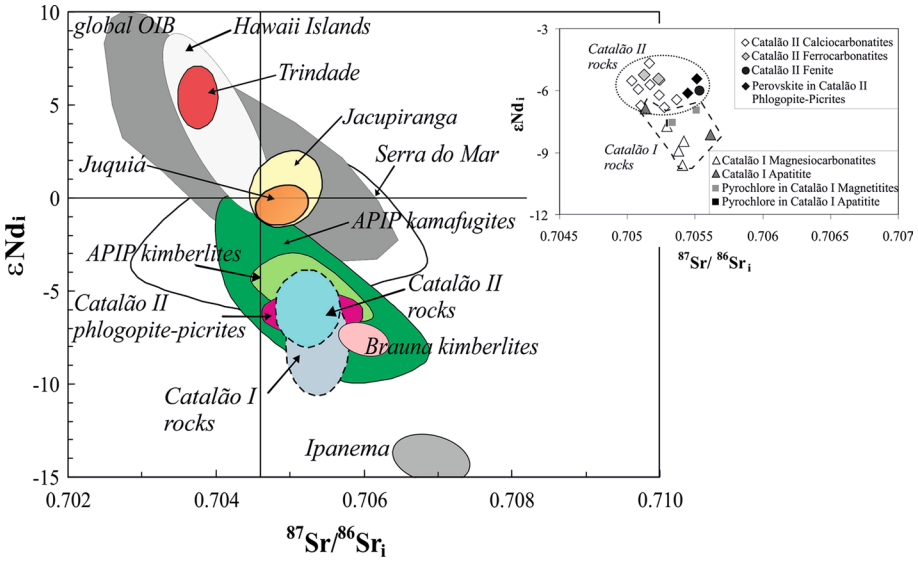

Fig. 9 εNd_i vs. $^{87}Sr/^{86}Sr_i$ diagram for the new isotopic data from Catalão II and Catalão I complexes. Catalão I lamprophyre is taken from Gomes and Comin-Chiaramonti (2005). The Catalão I compositional field is from Cordeiro et al. (2010, 2011a, b). APIP kimberlite and kamafugite fields are according to Gibson et al. (1995), Carlson et al. (1996), Thompson et al. (1998), Araújo et al. (2001), Gomes and Comin-Chiaramonti (2005) and Guarino et al. (2013). The Catalão II phlogopite-picrite field is taken from Guarino et al. (2013), Gibson et al. (1995) and Gomes and Comin-Chiaramonti (2005). Brauna kimberlite field is taken from Donatti-Filho et al. (2013). The isotopic compositions of the Ipanema (Guarino et al. 2012), Jacupiranga (Huang et al. 1995) and Juquiá (Beccaluva et al. 1992) carbonatites are shown for comparison. The Trindade field is from Halliday et al. (1992). The Serra do Mar field is based on Thompson et al. (1998), Bennio et al. (2002), Lustrino et al. (2003) and Brotzu et al. (2005, 2007). Global OIB and Hawaii Islands data are from Jackson et al. (2012) and references therein

($\delta^{13}C = -6.16$ to -6.03 ‰). In syenite fenite, phlogopite has $\delta^{18}O = 8.23$ ‰ and clinopyroxene has $\delta^{18}O = 6.58$–6.70 ‰. In the Catalão I complex, calcite in a magnesiocarbonatite has $\delta^{18}O$ of 10.75 ‰ and $\delta^{13}C$ of -5.79 ‰, and magnetite in magnetitite and phlogopite in apatitite have $\delta^{18}O = 7.10$–7.17 ‰ and $\delta^{18}O = 6.13$–6.29 ‰, respectively.

The coupled carbon and oxygen isotopes of calcite from the Catalão II calcio- and ferrocarbonatites plot in the "primary igneous carbonatite" field (Fig. 12a) (Taylor et al. 1967; Keller and Hoefs 1995), whereas the Catalão I magnesiocarbonatites have slightly higher $\delta^{18}O$. The Catalão I magnesiocarbonatite data are similar to those reported from Catalão I dolomite carbonatites (Cordeiro et al. 2011a). The Catalão II carbon and oxygen compositions are distinct from limestones of Precambrian ($\delta^{18}O = 15$–25 ‰, $\delta^{13}C = -5$ to 12 ‰) and Phanerozoic ($\delta^{18}O = 21$–31 ‰, $\delta^{13}C = -3$ to 7 ‰) ages (Bell 2005).

The $\delta^{18}O$ of calcite of the Catalão II carbonatites shows limited variation with depth (from -79.2 to -400 m), ranging between 8.45 and 9.48 ‰. The Catalão II data are in or close to the primary mantle values in the diagram $^{87}Sr/^{86}Sr_i$ versus $\delta^{18}O$ (Fig. 12b), whereas Catalão I data on magnesiocarbonatites likely reflect hydrothermal alteration of carbonates.

Age determinations for Catalão II and Catalão I complexes and their significance

New in situ U–Pb ages on baddeleyite (ZrO_2) of magnetitites (C1C13, C1C20) and apatitite (C1C22) of Catalão I complex (Fig. 13, Supplementary Fig. 3; Supplementary Data) are reported in Table 2 and shown in Fig. 1. The U–Pb baddeleyite ages of Catalão I range from 78 ± 1 to 81 ± 4 Ma. The new U–Pb ages for Catalão I are slightly younger (78 ± 1 to 81 ± 4 Ma) than the previous ages (85.0 ± 6.9 Ma; Sonoki and Garda 1988).

New in situ U–Pb ages on perovskite for Catalão II phlogopite-picrites (82 ± 3 Ma, 83 ± 4 Ma and 90 ± 4 Ma) are reported in Guarino et al. (2013). The data obtained for Catalão II place the age in the 82 ± 3 and 83 ± 4 Ma interval, similar to the previous age (83 Ma; Machado 1991) The oldest age obtained for Catalão II phlogopite-picrite (90 ± 4 Ma) can be the result of several possibilities: (a) perovskites are inherited crystals; (b) perovskite indicate an older emplacement age of this complex, still within the ranges of the APIP ages (91–71 Ma; Guarino et al. 2013 and references therein), and (c) perovskites are xenocrysts crystallized under open-system conditions (cf. Wu et al. 2010a, b; Cucciniello et al. 2010 and references therein).

Table 2 U–Pb ages, Lu–Hf and Rb–Sr isotopes on minerals and whole rocks of the Catalão II and Catalão I rocks

Rock	Locality	References	Sample	Borehole no.	Depth below ground-level	Analyses on	Type of analyses	$^{206}Pb/^{238}U$ weighted ages (Ma)	$^{176}Lu/^{177}Hf$	$^{176}Hf/^{177}Hf$	2SD	$\varepsilon_{Hf}(t)$	$^{176}Hf/^{177}Hf_i$	$\varepsilon_{Hf(i)}$	T_{DM} Hf
Phl-Picrite	Catalão II	Guarino et al. (2013)	C2A8	C3B2 (A)	137.8	Perovskite	SIMS	83 ± 4							
Phl-Picrite	Catalão II	Guarino et al. (2013)	C2A18	C3B2 (A)	290.1	Perovskite	SIMS	90 ± 4							
Phl-Picrite	Catalão II	Guarino et al. (2013)	C2B23	C3B1 (B)	368.8	Perovskite	SIMS	82 ± 3							
Magnetitite	Catalão I	This work	C1C13	49E 33 N	338.3	Baddeleyite	Laser	78 ± 1	0.000044	0.282493	0.000090	−8.1	0.28249	−10.3	1.0
Magnetitite	Catalão I	This work	C1C20	49E 33 N	497.6	Baddeleyite	Laser	81 ± 4	0.000042	0.282480	0.000090	−8.6	0.28248	−10.8	1.1
Apatitite	Catalão I	This work	C1C22	49E 33 N	510.0	Baddeleyite	Laser	80 ± 5	0.000058	0.282477	0.000090	−8.7	0.28248	−10.9	1.1
								$^{87}Rb/^{86}Sr$	$^{87}Sr/^{86}Sr$	2SD	$^{147}Sm/^{144}Nd$	$^{143}Nd/^{144}Nd$	2SD	$^{87}Sr/^{86}Sr_i$	$^{143}Nd/^{144}Nd_i$	$\varepsilon_{Nd(i)}$	T_{DM} Nd
CaCc	Catalão II	This work	C2A2	C3B2 (A)	79.2	Whole-Rock		0.014752	0.705256	0.000058	0.0736	0.5123	0.000013	0.70524	0.51225	−5.5	0.7
Syenite	Catalão II	This work	C2A6	C3B2 (A)	109.7	Whole-Rock		0.459553	0.706069	0.000040	0.0816	0.5123	0.000010	0.70553	0.51223	−6.0	0.8
Phl-Picrite	Catalão II	Guarino et al. (2013)	C2A8	C3B2 (A)	137.8	Perovskite		0.001530	0.705450	0.000060	0.0694	0.5123	0.000013	0.70544	0.51222	−6.1	0.9
Phl-Picrite	Catalão II	Guarino et al. (2013)	C2A8	C3B2 (A)	137.8	Whole-Rock		0.494344	0.705714	0.000048	0.0984	0.5123	0.000011	0.70553	0.51221	−6.2	0.9
Phl-Picrite	Catalão II	Guarino et al. (2013)	C2A10	C3B2 (A)	161.2	Whole-Rock		0.911745	0.706187	0.000097	0.0837	0.5122	0.000013	0.70531	0.51223	−5.9	0.8
CaCc	Catalão II	This work	C2A15	C3B2 (A)	271.2	Whole-Rock		0.000579	0.705164	0.000028	0.0813	0.5123	0.000012	0.70516	0.51229	−4.7	0.7
CaCc	Catalão II	This work	C2A17	C3B2 (A)	287.0	Whole-Rock		0.001446	0.705037	0.000036	0.0851	0.5123	0.000011	0.70503	0.51225	−5.5	0.8
Phl-Picrite	Catalão II	Guarino et al. (2013)	C2A18	C3B2 (A)	290.1	Whole-Rock		0.480168	0.705727	0.000029	0.0974	0.5123	0.000013	0.70557	0.51223	−5.8	0.9
CaCc	Catalão II	This work	C2A19	C3B2 (A)	314.0	Whole-Rock		0.015041	0.705288	0.000051	0.0877	0.5122	0.000015	0.70527	0.51218	−6.8	0.9
CaCc	Catalão II	This work	C2A20	C3B2 (A)	320.0	Whole-Rock		0.004628	0.705088	0.000039	0.0846	0.5123	0.000013	0.70508	0.51223	−5.9	0.8
CaCc	Catalão II	This work	C2A21	C3B2 (A)	324.8	Whole-Rock		0.020537	0.705260	0.000054	0.0904	0.5123	0.000011	0.70524	0.51221	−6.2	0.9

Table 2 continued

							$^{87}Rb/^{86}Sr$	$^{87}Sr/^{86}Sr$	2SD	$^{147}Sm/^{144}Nd$	$^{143}Nd/^{144}Nd$	2SD	$^{87}Sr/^{86}Sr_i$	$^{143}Nd/^{144}Nd_i$	$\varepsilon_{Nd(i)}$	T_{DM} Nd
CaCc	Catalão II	This work	C2B17	C3B1 (B)	308.5	Whole-Rock	0.001157	0.705169	0.000034	0.0869	0.5123	0.000013	0.70517	0.51224	−5.7	0.8
FeCc	Catalão II	This work	C2B18	C3B1 (B)	312.9	Whole-Rock	0.080454	0.705217	0.000045	0.0878	0.5123	0.000010	0.70512	0.51226	−5.2	0.8
CaCc	Catalão II	This work	C2B19	C3B1 (B)	328.5	Whole-Rock	0.016198	0.705117	0.000044	0.0873	0.5122	0.000012	0.70510	0.51219	−6.7	0.9
CaCc	Catalão II	This work	C2B22	C3B1 (B)	354.0	Whole-Rock	0.000579	0.705362	0.000042	0.1034	0.5123	0.000013	0.70536	0.51220	−6.4	0.9
Phl-Picrite	Catalão II	Guarino et al. (2013)	C2B23	C3B1 (B)	368.8	Perovskite	0.006000	0.705540	0.000060	0.0677	0.5123	0.000080	0.70551	0.51225	−5.4	0.8
Phl-Picrite	Catalão II	Guarino et al. (2013)	C2B23	C3B1 (B)	368.8	Whole-Rock	0.734865	0.705802	0.000057	0.0816	0.5123	0.000010	0.70599	0.51219	−6.7	0.8
FeCc	Catalão II	This work	C2B24	C3B1 (B)	400.0	Whole-Rock	0.015041	0.705247	0.000048	0.0735	0.5123	0.000011	0.70523	0.51225	−5.4	0.7
Magnetitite	Catalão I	This work	C1A5	F72	100.0	Whole-Rock	0.029771	0.705168	0.000075	0.0800	0.5122	0.000007	0.70513	0.51218	−6.9	0.8
MgCc	Catalão I	This work	C1B10	3E 19 N	175.0	Whole-Rock	0.000579	0.705379	0.000037	0.1080	0.5121	0.000012	0.70538	0.51208	−8.9	1.1
MgCc	Catalão I	This work	C1C4	49E 33 N	130.0	Whole-Rock	0.000579	0.705293	0.000067	0.0913	0.5122	0.000011	0.70529	0.51214	−7.7	0.9
MgCc	Catalão I	This work	C1C12B	49E 33 N	312.8	Whole-Rock	0.002810	0.705410	0.000037	0.1616	0.5121	0.000012	0.70541	0.51204	−9.6	1.9
MgCc	Catalão I	This work	C1C14	49E 33 N	357.4	Whole-Rock	0.002729	0.705419	0.000050	0.1032	0.5122	0.000010	0.70542	0.51210	−8.5	1.1
Magnetitite	Catalão I	This work	C1C13	49E 33 N	338.3	Pyrochlore	0.000720	0.705540	0.000080	0.0716	0.5122	0.000040	0.70551	0.51218	−6.9	0.8
Magnetitite	Catalão I	This work	C1C20	49E 33 N	497.6	Pyrochlore	0.000110	0.705330	0.000030	0.0668	0.5122	0.000100	0.70531	0.51214	−7.6	0.8
Apatitite	Catalão I	This work	C1C22	49E 33 N	510.0	Pyrochlore	0.000040	0.705330	0.000060	0.0637	0.5122	0.000060	0.70533	0.51215	−7.5	0.8
Apatitite	Catalão I	This work	C1C22	49E 33 N	510.0	Whole-Rock	0.015899	0.705630	0.000091	0.0689	0.5122	0.000017	0.70561	0.51212	−8.1	0.8

Phl-Picrite phlogopite-picrite; *CaCc* calciocarbonatite; *FeCc* ferrocarbonatite; *MgCc* magnesiocarbonatite

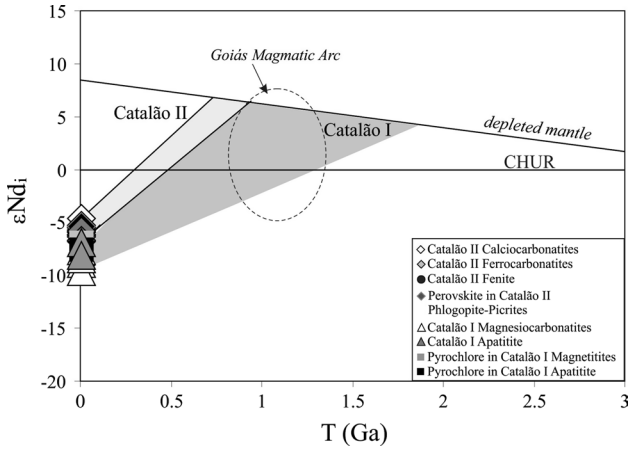

Fig. 10 εNd_i vs time diagram for Catalão II and Catalão I samples investigated in this study. The compositional field of meta-igneous rocks of the Goiás Magmatic Arc is shown for comparison (data from Pimentel et al. 1996)

Discussion

Mineralogical and geochemical evidence of igneous cumulates

The complex mineralogical assemblages linked to the cumulitic texture of the Catalão II calciocarbonatites, ferrocarbonatites, apatitites, magnetitites and phlogopitites make difficult to establish the crystallization relationships between the different minerals. Carbonates, apatite and phlogopite are ubiquitous, followed by pyrochlore and magnetite, with other accessory minerals such as REE-carbonates, wadeite, baddeleyite, clinopyroxene and amphibole. The possible order of crystallization in the Catalão II cumulitic rocks, based on petrographic study, is the co-crystallization of apatite–magnetite–phlogopite–pyrochlore minerals (e.g. phlogopite encloses apatite or vice versa). The carbonates crystallized after them. The predominant carbonates (e.g. calcite) enclosed other minerals, while minor carbonates (e.g. REE-carbonates) show an interstitial or are enclosed in calcite grains. Clinopyroxene and amphibole in the carbonatites are anhedral, indicating that they could be inherited xenocrystals, as are the wadeite crystals.

The bimodal composition of pyrochlore (Fig. 6) likely suggests equilibrium with magmas of variable composition, and the presence of complex chemical patterns (Fig. 7) suggests rhythmic/crystallographically controlled zoning may be due to refilling magma chambers by new influx of incompatible element-rich carbonatitic magmas; the convolute zoning can also represent dissolution–reprecipitation processes, which may or may be not related to refilling magma chambers. Pyrochlore and apatite have similar F; their wide distribution and notable amount in these rocks testify high volatile concentration in all new influx of magmas. The concentration of SrO is higher in calciocarbonatites (up to 2.2 wt%) than in the non-carbonatic rocks (SrO < 1.4 wt%), due to the preferential partitioning of strontium in the carbonates. The wide compositional

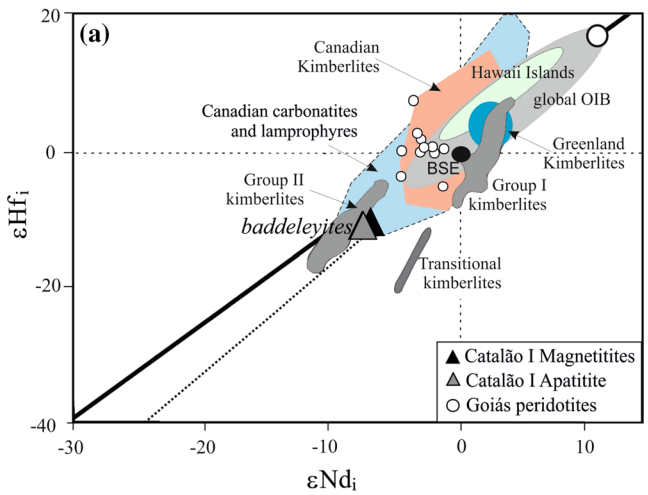

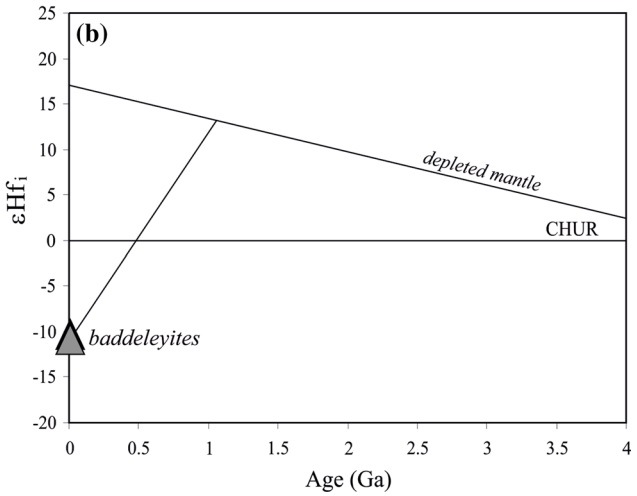

Fig. 11 **a** εHf_i vs. εNd_i diagrams for the Catalão I samples (diagram modified after Nowell et al. 2004). The fields of Group I, Group II and Transitional kimberlites (Table 1; cf. Nowell et al. 2003a, b), Goiás peridotite xenoliths hosted by kamafugites (Carlson et al. 2007), Canadian kimberlites (Kopylova et al. 2009; Tappe et al. 2013, 2014), Canadian carbonatites and lamprophyres (Bizimis et al. 2003; Tappe et al. 2007, 2008) and Greenland kimberlites (kimberlites/ailikites and associated carbonatites, Gaffney et al. 2007; Tappe et al. 2011) fields are shown for comparison. Global OIB and Hawaii Islands fields are from Jackson et al. (2012) and references therein. **b** εHf_i vs time diagram for baddeleyite of Catalão I apatitite and magnetitites. Note: εNd_i utilized is that of host rocks; decay constant (λ) of 1.865×10^{-11} (Scherer et al. 2006); depleted mantle values: $^{176}Lu/^{177}Hf = 0.0384$ and $^{176}Hf/^{177}Hf = 0.28325$ (Blichert-Toft and Albarede 1997)

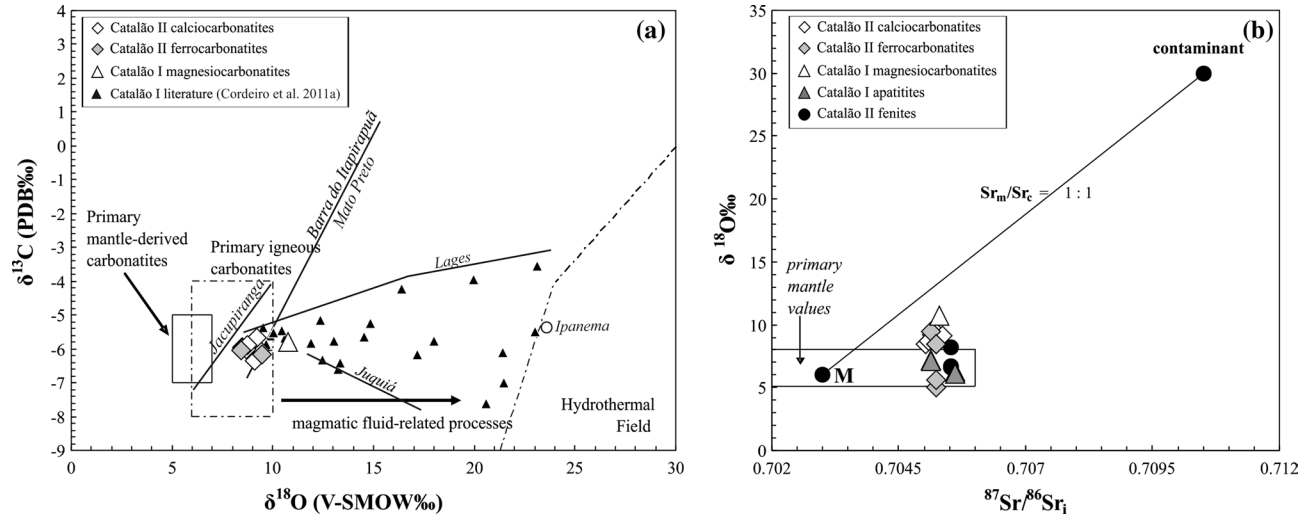

Fig. 12 **a** Plot of $\delta^{18}O$ ‰ (V-SMOW) vs. $\delta^{13}C$ ‰ (PDB) for Catalão II and Catalão I carbonatites. *Box* for primary igneous carbonatites is from Keller and Hoefs (1995) and Taylor et al. (1967). Catalão I literature is dolomite carbonatite investigated by Cordeiro et al. (2011a) and is reported for comparison (*black triangles*). Jacupiranga, Juquiá, Lages, Mato Preto, Barra do Itapirapuã trends are taken from Comin Chiaramonti et al. (2005a, b). The value of the Ipanema carbonatite is taken from Guarino et al. (2012). **b** $^{87}Sr/^{86}Sr_i$ versus $\delta^{18}O$ ‰ (V-SMOW) mixing diagram (cf. James 1981) for the rocks from the Catalão II and I complexes. End members: Brazilian crust and groundwater isotopic compositions are from Garland et al. (1995) and Taylor (1978), respectively

Table 3 Analyses of O and C isotopes on minerals in the Catalão II and Catalão I rocks

Rock	Site	Sample	Borehole no.	Depth below groundlevel	Mineral	$\delta^{18}O$ ‰ (V-SMOW)	$\delta^{13}C$ ‰ (PDB)
CaCc	Catalão II	C2A2	C3B2 (A)	79.2	Cal	9.36	−6.03
Syenite	Catalão II	C2A6	C3B2 (A)	109.7	Cpx	6.58	
Syenite	Catalão II	C2A6	C3B2 (A)	109.7	Cpx	6.70	
Syenite	Catalão II	C2A6	C3B2 (A)	109.7	Phl	8.23	
CaCc	Catalão II	C2A15	C3B2 (A)	271.2	Cal	9.21	−5.68
CaCc	Catalão II	C2A17	C3B2 (A)	287.0	Cal	8.49	−5.96
CaCc	Catalão II	C2A19	C3B2 (A)	314.0	Cal	8.68	−5.97
CaCc	Catalão II	C2A20	C3B2 (A)	320.0	Cal	8.70	−5.95
CaCc	Catalão II	C2A21	C3B2 (A)	324.8	Cal	8.46	−5.97
CaCc	Catalão II	C2B17	C3B1 (B)	308.5	Cal	8.69	−6.00
FeCc	Catalão II	C2B18	C3B1 (B)	312.9	Cal	9.48	−6.16
CaCc	Catalão II	C2B19	C3B1 (B)	328.5	Cal	8.74	−5.90
CaCc	Catalão II	C2B22	C3B1 (B)	354.0	Cal	9.13	−6.35
FeCc	Catalão II	C2B24	C3B1 (B)	400.0	Cal	8.45	−6.03
Magnetitite	Catalão I	C1A5	F72	100.0	Op	7.17	
Magnetitite	Catalão I	C1A5	F72	100.0	Op	7.10	
MgCc	Catalão I	C1C4	49E 33 N	130.0	Cal	10.75	−5.79
Apatitite	Catalão I	C1C22	49E 33 N	510.0	Phl	6.29	
Apatitite	Catalão I	C1C22	49E 33 N	510.0	Phl	6.13	

CaCc calciocarbonatite; *FeCc* ferrocarbonatite; *MgCc* magnesiocarbonatite, *Cal* calcite; *Phl* phlogopite; *Op* opaque mineral; *Cpx* clinopyroxene

variability of the carbonates (being Ca-, Ba-, Sr- and REE-bearing) indicates saturation with different carbonates at different crystallization stages in the magma reservoir.

The Catalão II calciocarbonatites and ferrocarbonatite (C2B18) and some Catalão I magnesiocarbonatites show troughs at Zr and Hf in the primitive mantle-normalized

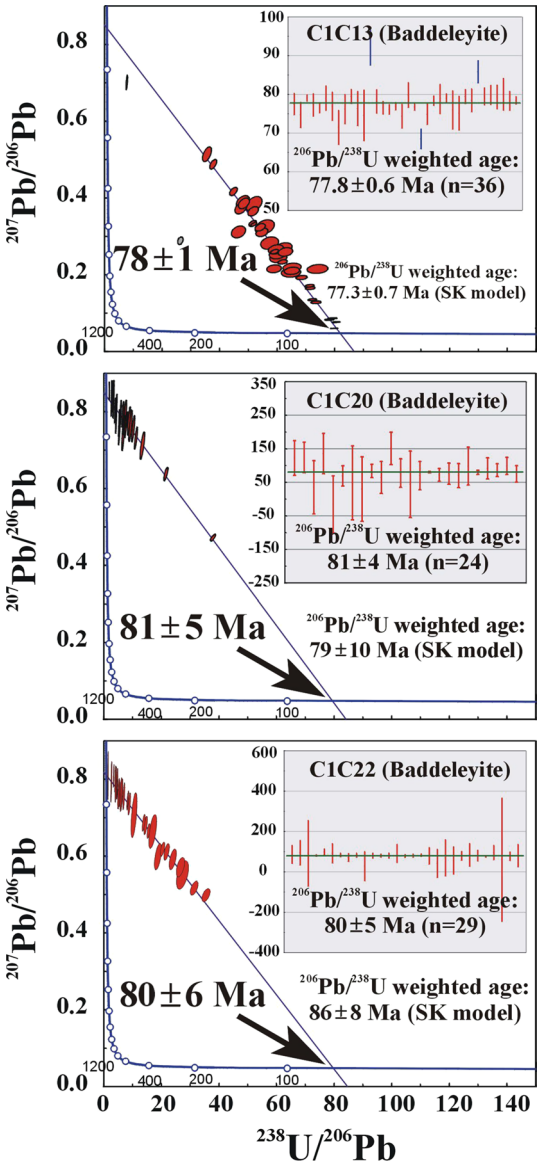

Fig. 13 U–Pb ages obtained by LA-ICP-MS from baddeleyite of two magnetitites (C1C13 and C1C20) and an apatitite (C1C22) of the Catalão I complex

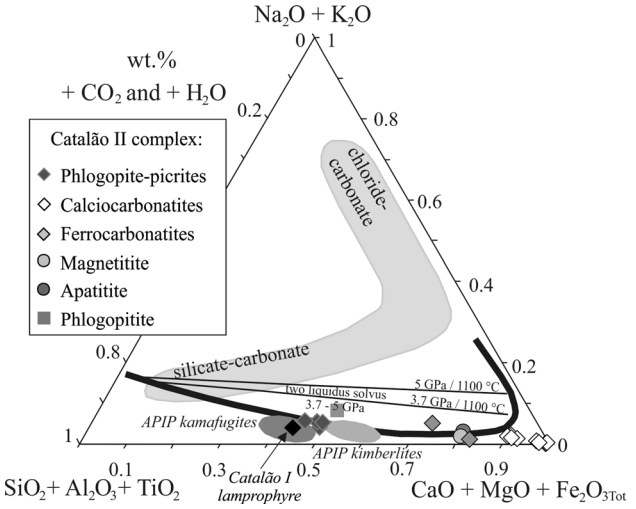

Fig. 14 Pseudoternary diagram (SiO_2 + Al_2O_3 + TiO_2 – CaO + MgO + Fe_2O_{3Tot} – Na_2O + K_2O) showing the chemical composition of rocks from the Catalão II complex (modified after Grassi and Schmidt 2010). The *thick line* represents the limit of liquid miscibility gap at 1100 °C, 3.7–5 GPa (Thomsen and Schmidt 2008). The APIP kimberlites and kamafugites fields and Catalão I lamprophyre (Gomes and Comin-Chiaramonti 2005) are reported for comparison (Guarino et al. 2013)

patterns, typical of magmatic carbonatites (cf. Woolley and Kempe 1989). The Catalão II ferrocarbonatite (C2B24) has less marked troughs at Zr and Hf that can be related to the presence of small amounts of modal wadeite ($K_2ZrSi_3O_9$) or indicates a late-stage carbothermal residual magma (Mitchell 2005). The troughs at Zr and Hf, typical of magmatic carbonatites worldwide, are less marked or absent in some Catalão I magnesiocarbonatites (sample C1C14) and in dolomite carbonatites of Cordeiro et al. (2010).

The typical troughs at Zr and Hf in carbonatites are thought to be due to the strong selective enrichment in large-ion lithophile elements (Rb, Sr, Ba), Th, U, rare-earth elements over high field strength elements (such as Hf, Zr and Ti) (e.g. Green et al. 1992; Yaxley and Green 1996; Walter et al. 2008). In addition, there is no correlation between Zr concentration and Zr/Hf ratio of carbonatites and associated silicate rocks. This is ultimately caused by source effects rather than fractional crystallization of a specific phase (Andrade et al. 2002; Chakhmouradian 2006 and references therein).

The mantle-normalized patterns of non-carbonatic rocks (apatitite and magnetitites) in Catalão II and Catalão I complexes are generally similar to those of the Catalão II phlogopite-picrites and Catalão I lamprophyre, which are interpreted to represent the most primitive liquid composition in these complexes (Guarino et al. 2013).

The Catalão II cumulitic rocks have similar Sr–Nd isotopes of the APIP kimberlites, kamafugites and phlogopite-picrites (Fig. 9), suggesting limited isotopic heterogeneity in the sources of the APIP mantle-derived magmas. The distribution of Nd isotope data in the diagram εNd versus time (Fig. 10) indicates that the Catalão II rocks are different from those of the Goiás Province. The coupled carbon and oxygen isotopes of calcite from the Catalão II calcio- and ferrocarbonatites plot in the "primary igneous carbonatite" field (Fig. 12a). Carbon ($\delta^{13}C = -6.35$ to -5.68 ‰) isotopic data suggest a mantle origin for the carbon of the carbonatites.

The petrological characteristics of the magma in the Catalão II intrusion

The liquids that filled the Catalão II intrusion were likely silica-poor and had a Ca-rich ultramafic composition, rich in K, volatiles, HFSE and REE. These liquids were able to crystallize carbonates, apatite, phlogopite, pyrochlore and magnetite, and other accessory minerals (e.g. REE-carbonates, wadeite, baddeleyite), giving rise to the cumulate compositions reported above. The significant variation in the chemical, modal and mineralogical compositions in Catalão II rocks could be explained through differential settling of the heavy phases (magnetite, apatite, pyrochlore and sulphides) in a magma chamber repeatedly filled by influx of carbonatite magma. Due to this repeated process, the crystallization sequence cannot be identified with certainty (see Fig. 2). This refilling is reflected in the rhythmic cumulates found at different depths during the emplacement of magma that filled the Catalão II intrusion.

It is not clear whether the carbonatite liquids that filled the Catalão intrusion represent conjugate compositions of the phlogopite-picrite dykes (e.g. Table 1a,b; Fig. 8; Supplementary Fig. 5). The chemical composition of Catalão II cumulitic rocks is plotted into the pseudoternary system $SiO_2 + Al_2O_3 + TiO_2 - CaO + MgO + Fe_2O_{3Tot} - Na_2O + K_2O$ (Fig. 14) in the presence of H_2O and CO_2 (cf. Grassi and Schmidt 2010). In this diagram, the Catalão II phlogopite-picrites plot close to APIP kimberlite and kamafugite fields and the Catalão I lamprophyre. These rocks plot generally below the curve representing the limit of liquid miscibility gap at 1100 °C (3.7–5 GPa), consistent with the pressure of 3–5 GPa estimated for the APIP rocks (Guarino et al. 2013), based on MgO/CaO vs. SiO_2/Al_2O_3 diagram (Gudfinnsson and Presnall 2005). The Catalão II cumulitic rocks fall outside the liquid immiscibility field, again suggesting that they may not be representatives of carbonatitic liquid compositions. The phlogopite-rich rocks and one ferrocarbonatite plot below this curve, probably due to their high K_2O concentrations (7.1 wt% in phlogopitite and 3.4 wt% in ferrocarbonatite).

The ultramafic lamprophyre formation, association and genetic model for the APIP magmatism

The Catalão II phlogopite-picrites and Catalão I lamprophyre, together with kimberlites and kamafugites, are part of APIP magmatism that features by strongly silica undersaturated magmas, with high concentration of CaO, volatiles (CO_2 and H_2O) and low Na_2O. These features are typical of melting a volatile-rich, Na-poor peridotitic source assemblage metasomatized by phlogopite- and carbonate-rich veins (Guarino et al. 2013 and references therein). Partial melting of such a carbonated peridotite can produce low-SiO_2 melts (e.g. Gudfinnsson and Presnall 2005; Dasgupta et al. 2007). The Catalão II phlogopite-picrites, as well as the APIP kimberlites and kamafugites, are interpreted to result from low-degree partial melting ($f = 0.5$–2 %) of a mantle source consisting of a carbonated incompatible element-enriched lherzolite with phlogopite-rich veins (Guarino et al. 2013).

The APIP phlogopite-picrites and lamprophyres are associated with carbonatites at Tapira, Catalão I, Catalão II, Araxá and Salitre (Gibson et al. 1995; Morbidelli et al. 1997; Traversa et al. 2001; Gomes and Comin-Chiaramonti 2005; Guarino et al. 2013). In this way, the association scheme proposed by Woolley and Kjarsgaard (2008a, b) where APIP carbonatites are associated only with *"ultramafic cumulates"* can be reconsidered. We propose that the APIP carbonatites are also associated with *"lamprophyres"*.

Three main models have been hypothesized for the petrogenesis of the APIP magmatism. Two models are based on the postulated presence of mantle plumes, while the third considers the partial melting of metasomatized lithospheric mantle. The first model, based on the common "Dupal" Sr–Nd–Pb isotopic composition of the Brazilian alkaline rocks, has highlighted a genetic link with some South Atlantic OIB and seamounts with Dupal geochemical signatures (e.g. Walvis Ridge and Rio Grande Rise), proposing that the source of the APIP rocks was modified by the Tristan da Cunha hot spot at ~130 Ma (Bizzi et al. 1995). The second model assumed a SE-directed decrease in the age of the igneous activity, from ~90 Ma in the northwesternmost Iporá Province towards ~80 Ma in the APIP and finally ~60 Ma in the south-easternmost sectors of the Serra do Mar Igneous Province, caused by a hotspot track, whose present-day products are represented by Trindade–Martin Vaz archipelago (Gibson et al. 1995; Thompson et al. 1998; Sgarbi et al. 2004). The third model is based upon different lithospheric mantle sources in the genesis of the Goiás and Alto Paranaíba alkaline rocks (Carlson et al. 1996, 2007). Guarino et al. (2013) highlighted the Sr–Nd isotopic ($^{87}Sr/^{86}Sr_i = 0.70431$–$0.70686$; $\varepsilon Nd_i = -6.7$ to -3.9) similarity between the 91- and 71-Ma-old APIP rocks and 642-Ma-old Brauna kimberlites ($^{87}Sr/^{86}Sr_i = 0.7045$–$0.7063$ and $\varepsilon Nd_i = -5.8$ to -8.1; Donatti-Filho et al. 2013), situated in the north-east part of the São Francisco craton, testifying limited isotopic changes in the mantle of south-eastern Brazil since Late Precambrian. The ages of APIP rocks (91–71 Ma; Guarino et al. 2013) similar to those of the Goiás Province (~91–90 Ma) are not evidence of a hot-spot track, testifying an almost coeval magma production in the Goias and Alto Paranaiba provinces, located more than 400 km apart each other. The volcanic activity lasted in the APIP probably up to Late Cretaceous (71 Ma; Sonoki and Garda 1988) or Palaeocene (~61 Ma; Read

et al. 2004 and references therein). In addition, the Sr–Nd isotope composition of the present-day products of the Trindade plume (Halliday et al. 1992) is totally different from that of the APIP rocks (Fig. 9). The exotic chemical composition of the magmas of the APIP province requires low to very low degrees of partial melting and could be interpreted as the effect of chemically and mineralogically heterogeneous, low-melting mantle source rich in carbonates, potassium and hydrous phases, acquired during the Brasiliano orogenic cycle, when the Amazonian and São Francisco cratons collided. As a consequence, the involvement of a thermal perturbation caused by the presence of a hotspot or a mantle plume could not be required. Melting can be the consequence of rifting episodes.

Relationships with other Brazilian carbonatite associations

The Mesozoic alkaline-carbonatitic complexes in southern Brazil are located around the border of the Paraná Basin. Catalão I, Catalão II, Tapira and Araxá in the APIP, together with Ipanema, in the Ponta Grossa Arch Magmatic Province, and Anitapolis, Juquiá and Jacupiranga are the most prominent alkaline-carbonatitic complexes that border the Paraná Basin (Ruberti et al. 2005; Fig. 1). Within these complexes, calciocarbonatites are the most common variety, followed by magnesio- and minor ferrocarbonatites. The carbonatites are associated with ultramafic cumulates and fenitized rocks (Woolley and Kjarsgaard 2008a, b). The Alto Paranaíba complexes having carbonatitic rocks (Araxá, Salitre, Catalão I and Catalão II) also have apatitites, magnetitites and phlogopitites, as well as dunites and wehrlites. The Tapira carbonatites are associated with Ca-rich, Na-poor melilitite ± melilitolite ± ultramafic cumulate rocks (e.g. clinopyroxenites, "bebedourites" and "salitrites"). On the other hand, the carbonatites roughly coeval with the Paraná flood basalt province (e.g. Juquiá, Anitapolis, Lages and Jacupiranga) are associated with nephelinite ± melteigite/ijolite/urtite ± ultramafic cumulate rocks and subordinate melilite- and nepheline-bearing intrusive rocks (e.g. Beccaluva et al. 1992; Traversa et al. 1996; Ruberti et al. 2005). These different rock associations provide compelling evidence that the carbonatites of southern Brazil are the products of alkaline magmas of contrasting composition, ranging from Na-rich (i.e. olivine nephelinites, olivine melilitites, basanites) in southernmost Brazil to nearly Na-free compositions (ultrapotassic/kamafugitic) in the APIP.

Differences in the source region of the alkaline magmatism that formed the APIP and the alkaline rocks in southernmost Brazil are also visible in the marked Sr–Nd isotopic differences between Catalão and the Juquiá–Jacupiranga–Ipanema carbonatites (Fig. 9). This difference is consistent with a heterogeneous lithospheric mantle source on a regional scale (e.g. Bizzi et al. 1995). In addition, the Hf isotope composition of the Catalão I magnetitites and apatitite is different from that of the Goiás peridotites (Carlson et al. 2007), indicating again marked isotopic heterogeneity in the mantle of the area. The Hf isotope differences between our data with global OIB and Hawaii Islands data indicate the absence of an asthenospheric or plume chemical component. Marked Hf isotope differences were also observed in the Greenland and Canadian kimberlite fields; on the other hand, the Catalão carbonatites plot at the lower isotopic range of the Canadian carbonatite–lamprophyre fields (Fig. 11). These features indicate a distinct petrogenesis for the various carbonatitic associations, characterized by primary magmas with sodic-to-ultrapotassic affinity, different compositions and different enrichment processes.

Conclusions

The new U–Pb ages for Catalão II place the age in the interval 82 ± 3 and 83 ± 4 Ma (Guarino et al. 2013) and between 78 ± 1 and 81 ± 4 Ma for Catalão I. The Catalão II carbonatitic complex formed through extensive accumulation processes that may have occurred at the bottom or borders of magma reservoirs repeatedly refilled by carbonatitic magma. The magnetitites and apatitites are not analogues of liquid compositions; rather, they formed after crystal accumulation process at the bottom of transient magma reservoirs. The geological complexity of the APIP area has influenced the emplacement of these cumulitic rocks as dykes in the Brasilia Belt. The strong geochemical similarity between Catalão II cumulitic rocks and phlogopite-picrites suggests a similar mantle source, which we interpret to be a carbonated phlogopite-rich peridotite, highly enriched in incompatible elements (HFSE and LILE). This mantle enrichment likely occurred in the Late Precambrian during the Brasilia Belt formation, as indicated by hafnium isotope and neodymium model age. The carbon isotopes of calcite of calcio- and ferrocarbonatites preserve the carbon mantle signatures without any input of Precambrian or Phanerozoic limestones. The new Sr–Nd isotopic ratios for the Catalão II rocks indicate similar radiogenic compositions as those of typical APIP rocks, such as kimberlites, kamafugites and phlogopite-picrites. New Hf isotope compositions indicate a long-term isolated source having low Lu/Hf ratios, which are difficult to reconcile with melting of asthenospheric or volatile-rich plume components.

Acknowledgments The authors dedicate this paper to the Late Prof. Giampaolo Macciotta, who taught us how to link Informatics and Geology. Thanks to the owners of the Catalão mine for the access to the borehole samples. The reviews of Guilherme de Oliveira Gonçalves, Sebastian Tappe and, especially, a patient anonymous reviewer were very useful for the preparation of a revised manuscript. We also thank the Editor in Chief Wolf-Christian Dullo and the Topic Editor Axel Gerdes. Roberto de' Gennaro and Sergio Bravi are thanked for their assistance in the microprobe and thin-section preparation. Pietro Brotzu and Lucio Morbidelli are gratefully thanked for their continuous support and advice over the years. We also gratefully thank Michele Lustrino and Marcello Serracino (IGAG, CNR) for their help with analytical work and useful discussions. Thanks are also due to FAPESP (Proc. 2013/18073-4) to C.B. Gomes and PRIN 2010–2011 (20107ESMX9_001) to L. Melluso.

References

Almeida FFM, De Brito Neves BB, Carneiro CDR (2000) The origin and evolution of the south American platform. Earth Sci Rev 50:77–111

Andrade FRDD, Moller P, Dulski P (2002) Zr/Hf in carbonatites and alkaline rocks: new data and a re-evaluation. Rev Bras Geociencias 32:361–370

Araújo ALN, Carlson RW, Gaspar JC, Bizzi LA (2001) Petrology of kamafugites and kimberlites from the Alto Paranaíba Alkaline Province, Minas Gerais, Brazil. Contrib Miner Petrol 142:163–177

Asprey LB (1976) The preparation of very pure F_2 gas. J Fluorine Chem 7:359–361

Barker DS (1996) Consequences of recycled carbon in carbonatites. Can Miner 34:373–387

Beccaluva L, Barbieri M, Born H, Brotzu P, Coltorti M, Conte AM, Garbarino C, Gomes CB, Macciotta G, Morbidelli L, Ruberti E, Siena F, Traversa G (1992) Fractional crystallization and liquid immiscibility processes in the alkaline-carbonatite complex of Juquiá (São Paulo, Brazil). J Petrol 33:1371–1404

Bell K (2001) Carbonatites: relationships to mantle plume activity. In: Ernst RE, Buchan KL (eds) Mantle plumes: their identification through time. Geol Soc Spec Pap 352:267–290

Bell K (2005) Carbonatites. In: Selley RC, Cocks LRM, Plimer IR (eds) Encyclopedia of geology. Elsevier, Amsterdam, pp 217–233

Bell K, Rukhlov AS (2004) Carbonatites from the Kola Alkaline Province: origin, evolution and source characteristics. In: Zaitsev A, Wall F (eds) Phoscorites and carbonatites from mantle to mine: the key example of the Kola Alkaline Province, vol 10. Miner Society, London, pp 421–455

Bell K, Simonetti A (2010) Source of parental melts to carbonatites: critical isotopic constraints. Miner Petrol 98:77–89

Bell K, Tilton GR (2001) Nd, Pb and Sr isotopic compositions of east African carbonatites: evidence for mantle mixing and plume inhomogeneity. J Petrol 42:1927–1945

Bell K, Tilton GR (2002) Probing the mantle: the story from carbonatites. EOS, Am Geophys Union 83:273–277

Bennio L, Brotzu P, Gomes CB, D'Antonio M, Lustrino M, Melluso L, Morbidelli L, Ruberti E (2002) Petrological, geochemical and Sr-Nd isotopic features of alkaline rocks from the Arraial do Cabo Frio peninsula (Southeastern Brazil). Period Miner 71:137–158

Biondi JC (2005) Brazilian mineral deposits associated with alkaline and alkaline-carbonatite complexes. In: Comin-Chiaramonti P, Gomes CB (eds) Mesozoic to Cenozoic alkaline magmatism in the Brazilian Platform. FAPESP, São Paulo, pp 707–750

Bizimis M, Salters VJM, Dawson JB (2003) The brevity of carbonatite sources in the mantle: evidence from Hf isotopes. Contrib Miner Petrol 145:281–300

Bizzarro M, Simonetti A, Stevenson RK, David J (2002) Hf isotope evidence for a hidden mantle reservoir. Geology 30:771–774

Bizzi LA, De Wit MJ, Smith CB, McDonald I, Armstrong RA (1995) Heterogeneous enriched mantle materials and Dupal-type magmatism along the SW margin of the São Francisco Craton, Brazil. J Geodyn 20:469–491

Blichert-Toft J, Albarede F (1997) Separation of Hf and Lu for high-precision isotope analysis of rock samples by magnetic sector-multiple collector ICP-MS. Contrib Miner Petrol 127:248–260

Boynton WV (1984) Cosmochemistry of the rare earth elements: meteorite studies. In: Henderson P (ed) Rare earth element geochemistry. Elsevier, Amsterdam, pp 63–114

Brod JA, Gibson SA, Thompson RN, Junqueira-Brod TC, Seer HJ, Moraes LC, Boaventura GR (2000) The kamafugite-carbonatite association in the Alto Paranaíba Igneous Province (APIP) southeastern Brazil. Rev Bras Geociencias 30:408–412

Brotzu P, Melluso L, D'Amelio F, Lustrino M (2005) Mafic/ultramafic potassic dykes and felsic intrusions of the Serra do Mar igneous province (SE-Brazil): a review. In: Comin-Chiaramonti P, Gomes CB (eds) Mesozoic to Cenozoic alkaline magmatism in the Brazilian Platform. EDUSP/FAPESP, São Paulo, pp 443–472

Brotzu P, Melluso L, Bennio L, Gomes CB, Lustrino M, Morbidelli L, Morra V, Ruberti E, Tassinari CCG, D'Antonio M (2007) Petrogenesis of the Cenozoic potassic alkaline complex of Morro de São João, southeastern Brazil. J South Am Earth Sci 24:93–115

Bulanova GP, Walter MJ, Smith CB, Kohn SC, Armstrong LS, Blundy J, Gobbo L (2010) Mineral inclusions in sub lithospheric diamonds from Collier 4 kimberlite pipe, Juína, Brazil: subducted protoliths, carbonated melts and primary kimberlite magmatism. Contrib Miner Petrol 160:489–510

Carlson RW, Esperança S, Svisero DP (1996) Chemical and Os isotopic study of Cretaceous potassic rocks from Southern Brazil. Contrib Miner Petrol 125:393–405

Carlson RW, Araújo ALN, Junqueira-Brod TC, Gaspar JC, Brod JA, Petrinovic IA, Hollanda MHBM, Pimentel MM, Sichel SE (2007) Chemical and isotopic relationships between peridotite xenoliths and mafic-ultrapotassic rocks from Southern Brazil. Chem Geol 242:418–437

Chakhmouradian AR (2006) High-field-strength elements in carbonatitic rocks: geochemistry, crystal chemistry and significance for constraining the sources of carbonatites. Chem Geol 235:138–160

Chartier F, Aubert M, Salmon M, Tabarant M, Tran BH (1999) Determination of erbium in nuclear fuels by isotope dilution thermal ionization mass spectrometry and glow discharge mass spectrometry. J Anal Atom Spectrom 14:1461–1465

Comin Chiaramonti P, Gomes CB, Censi P, Speziale S (2005a) Carbonatites from southeastern Brazil: a model for the carbon and oxygen isotope variations. In: Comin-Chiaramonti P, Gomes CB (eds) Mesozoic to Cenozoic alkaline magmatism in the Brazilian Platform. Edusp/Fapesp, São Paulo, pp 629–649

Comin Chiaramonti P, Gomes CB, Marques LS, Censi P, Ruberti E, Antonini P (2005b) Carbonatites from Southeastern Brazil: geochemistry, O–C, Sr–Nd–Pb isotopes and relationships with the magmatism from the Paraná-Angola-Namibia Province. In: Comin-Chiaramonti P, Gomes CB (eds) Mesozoic to Cenozoic alkaline magmatism in the Brazilian Platform. Edusp/Fapesp, São Paulo, pp 657–688

Cordeiro PFO, Brod JA, Dantas EL, Barbosa ESR (2010) Mineral chemistry, isotope geochemistry and petrogenesis of niobium-rich rocks from the Catalão I carbonatite-phoscorite complex, central Brazil. Lithos 118:223–237

Cordeiro PFO, Brod JA, Santos RV, Dantas EL, Oliveira CG, Barbosa ESR (2011a) Stable (C, O) and radiogenic (Sr, Nd) isotopes of carbonates as indicators of magmatic and post-magmatic processes of phoscorite-series rocks and carbonatites from Catalão I, central Brazil. Contrib Miner Petrol 161:451–464

Cordeiro PFO, Brod JA, Palmieri M, Oliveira CG, Barbosa ESR, Santos RV, Gaspar JG, Assis LC (2011b) The Catalão I niobium deposit, central Brazil: resources, geology and pyrochlore chemistry. Ore Geol Rev 41:112–121

Cucciniello C (2016) Tetra-Plot: a Microsoft Excel spreadsheet to perform tetrahedral diagrams. Period Miner 85(2):115–119

Cucciniello C, Langone A, Melluso L, Morra V, Mahoney JJ, Meisel T, Tiepolo M (2010) U-Pb Ages, Pb-Os isotope ratios, and Platinum-Group Element (PGE) composition of the west-central Madagascar flood basalt province. J Geol 118:523–541

D'Agrella-Filho MS, Trindade RIF, Tohver E, Janikian L, Teixeira W, Hall C (2011) Paleomagnetism and $^{40}Ar/^{39}Ar$ geochronology of the high-grade metamorphic rocks of the Jequié block, São Francisco Craton: atlantica, Ur and beyond. Precamb Res 185:183–201

Dasgupta R, Hirschmann MM, Smith ND (2007) Partial melting experiments of peridotite+ CO_2 at 3 GPa and genesis of alkalic ocean island basalts. J Petrol 48:2093–2124

Donatti-Filho JP, Tappe S, Oliveira EP, Heaman LM (2013) Age and origin of the Neoproterozoic Brauna kimberlites: melt generation within the metasomatized base of the São Francisco craton, Brazil. Chem Geol 353:20–36

Dubois JC, Retali G, Cesario J (1992) Isotopic analysis of rare earth elements by total vaporization of samples in thermal ionization mass spectrometry. Int J Mass Spectrom—Ion Process 120:163–177

Dunworth EA, Bell K (2001) The Turiy Massif, Kola Peninsula, Russia: isotopic and geochemical evidence for multi-source evolution. J Petrol 42:377–405

Ehrlich S, Gavrieli I, Dor LB, Halicz L (2001) Direct high-precision measurements of the $^{87}Sr/^{86}Sr$ isotope ratio in natural water, carbonates and related materials by multiple collector inductively coupled plasma mass spectrometry (MC–ICP–MS). J Anal Atom Spectrom 16:1389–1392

Fortunato G, Mumic K, Wunderli S, Pillonel L, Bosset JO, Gremand G (2004) Application of strontium isotope abundance ratios measured by MC–ICP–MS for food authentication. J Anal Atom Spectrom 19:227–234

Foster GL, Carter A (2007) Insights into the patterns and locations of erosion in the Himalaya—a combined fission-track and in situ Sm–Nd isotopic study of detrital apatite. Earth Planet Sci Lett 257:407–418

Foster GL, Vance D (2006) *In situ* Nd isotopic analysis of geological materials by laser ablation MC–ICP–MS. J Anal Atom Spectrom 21:288–296

Gaffney AM, Blichert-Toft J, Nelson BK, Bizzarro M, Rosing M, Albarede F (2007) Constraints on source-forming processes of West Greenland kimberlites inferred from Hf–Nd isotope systematics. Geochim Cosmochim Acta 71:2820–2836

Garland F, Hawkesworth CJ, Mantovani MSM (1995) Description and petrogenesis of the Paraná rhyolites, Southern Brazil. J Petrol 36:1193–1227

Gibson SA, Thompson RN, Leonardos OH, Dickin AP, Mitchell JG (1995) The Late Cretaceous impact of the Trindade mantle plume: evidence from large-volume, mafic, potassic magmatism in SE Brazil. J Petrol 36:189–229

Gomes CB, Comin-Chiaramonti P (2005) Some notes on the Alto Paranaíba igneous province. In: Comin-Chiaramonti P, Gomes CB (eds) Mesozoic to Cenozoic alkaline magmatism in the Brazilian Platform. EDUSP/FAPESP, São Paulo, pp 317–340

Grassi D, Schmidt MW (2010) Melting of carbonated pelites at 8-13 GPa: generating K-rich carbonatites for mantle metasomatism. Contrib Miner Petrol 162:169–191

Green HW, Adam J, Sie SH (1992) Trace element partitioning between silicate minerals and carbonatite at 25 kbar and application to mantle metasomatism. Miner Petrol 46:179–184

Guarino V, Azzone RG, Brotzu P, Gomes CB, Melluso L, Morbidelli L, Ruberti E, Tassinari CCG, Brilli M (2012) Magmatism and fenitization in the Cretaceous potassium-alkaline-carbonatitic complex of Ipanema São Paulo State, Brazil. Miner Petrol 104:43–61

Guarino V, Wu F-Y, Lustrino M, Melluso L, Brotzu P, Gomes CB, Ruberti E, Tassinari CCG, Svisero DP (2013) U-Pb ages, Sr-Nd-isotope geochemistry, and petrogenesis of kimberlites, kamafugites and phlogopite-picrites of the Alto Paranaíba Igneous Province, Brazil. Chem Geol 353:65–82

Gudfinnsson GH, Presnall DC (2005) Continuous gradations among primary carbonatitic, kimberlitic, melilititic, basaltic, picritic, and komatiitic melts in equilibrium with garnet lherzolite at 3–8 GPa. J Petrol 46:1645–1659

Guimarães HN, Weiss RA (2013) The complexity of the niobium deposits in the alkaline ultramafic intrusions Catalão I and II—Brazil. www.cbmm.com.br/portug/sources/techlib/science/pdfs/002A.pdf

Halliday AN, Davies GR, Lee D, Tommasini S, Paslick CR, Fitton JG, James DE (1992) Lead isotope evidence for young trace element enrichment in the oceanic upper mantle. Nature 359:623–627

Hoernle K, Tilton G, Le Bas MJ, Duggen S, Garbe-Schonberg D (2002) Geochemistry of oceanic carbonatites compared with continental carbonatites: mantle recycling of oceanic crustal carbonate. Contrib Miner Petrol 142:520–542

Huang YM, Hawkesworth CJ, van Calsteren PWC, McDermott F (1995) Geochemical characteristics and origin of the Jacupiranga carbonatites, Brazil. Chem Geol 119:79–99

Isnard H, Brennetot R, Caussignac C, Caussignac N, Chartier F (2005) Investigations for determination of Gd and Sm isotopic compositions in spent nuclear fuels samples by MC ICPMS. Int J Mass Spectrom 246:66–73

Jackson SE, Pearson NJ, Griffin WL, Belousova E (2004) The application of laser ablation inductively coupled plasma mass spectrometry to in situ U–Pb zircon geochronology. Chem Geol 211:47–69

Jackson MG, Weis D, Huang S (2012) Major element variations in Hawaiian shield lavas: source features and perspectives from global ocean island basalt (OIB) systematics. Geochem Geophys Geosyst 13:Q09009. doi:10.1029/2012GC004268

James DE (1981) The combined use of oxygen and radiogenic isotopes as indicators of crustal contamination. Ann Rev Earth Planet Sci 9:311–344

Keller J, Hoefs J (1995) Stable isotope characteristics of recent natrocarbonatites Oldoinyo Lengai. In: Bell K, Keller J (eds) Carbonatite volcanism: Oldoinyo Lengai and the petrogenesis of natrocarbonatites. Springer, Berlin, pp 113–123

Kogarko LN (2006) Enriched mantle reservoirs are the source of alkaline magmatism. In: Vladykin NV (ed) Deep-seated magmatism, its sources and plumes. Proceedings of the VI international workshop, Mirny Publishing House of the Inst of Geography SB RAS, pp 46–58

Kopylova MG, Nowell GM, Pearson DG, Markovic G (2009) Crystallization of megacrysts from protokimberlitic fluids: geochemical evidence from high-Cr megacrysts in the Jericho kimberlite. Lithos 112:284–295

Le Bas MJ (2008) Fenites associated with carbonatites. Can Miner 46:915–932

Leake BE, Woolley AR, Arps CES, Gilbert MC, Grice JD, Hawthorne FC, Kato A, Kisch AJ, Krivovichev VG, Linthout K, Laird J,

Mandarino JA, Maresch WV, Nickel EH, Schumacher JC, Smith DC, Stephenson NCN, Whittaker EJW, Youzhi G (1997) Nomenclature of amphiboles: report of the subcommittee on amphiboles of the international mineralogical association, commission on new minerals and minerals names. Can Miner 35:219–246

Lee WJ, Wyllie PJ (1994) Experimental data bearing on liquid immiscibility, crystal fractionation, and the origin of calcio-carbonatites and natrocarbonatites. Int Geol Rev 36:797–819

Lee WJ, Wyllie PJ (1996) Liquid immiscibility in the join $NaAlSi_3O_8$-$CaCO_3$ to 25 GPa and the origin of calciocarbonatite magmas. J Petrol 37:1125–1152

Lee WJ, Wyllie PJ (1997a) Liquid immiscibility between nephelinite and carbonatite from 2·5 to 1·0 GPa compared with mantle melt compositions. Contrib Miner Petrol 127:1–16

Lee WJ, Wyllie PJ (1997b) Liquid immiscibility in the join $NaAlSiO_4$-$NaAlSi_3O_8$-$CaCO_3$ at 10 GPa: implications for crustal carbonatites. J Petrol 38:1113–1135

Lee WJ, Wyllie PJ (1998) Petrogenesis of carbonatite magmas from mantle to crust, constrained by the system CaO–(MgO+ FeO*)–(Na_2O+ K_2O)–(SiO_2+ Al_2O_3+ TiO_2)–CO_2. J Petrol 39:495–517

Lee MJ, Lee JI, Garcia D, Moutte J, Williams CT, Wall F, Kim Y (2006) Pyrochlore chemistry from the Sokli phoscorite-carbonatite complex, Finland: implications for the genesis of phoscorite and carbonatite association. Geochem J 40:1–13

Locock AJ (2008) An Excel spreadsheet to recast analyses of garnet into end-member components, and a synopsis of the crystal chemistry of natural silicate garnets. Comput Geosci 34:1769–1780

Locock AJ (2014) An Excel spreadsheet to classify chemical analyses of amphiboles following the IMA 2012 recommendations. Comput Geosci 62:1–11

Lustrino M, Dallai L, Giordano R, Gomes CB, Melluso L, Morbidelli L, Ruberti E, Tassinari CCG (2003) Geochemical and Sr-Nd-O isotopic features of the Poços de Caldas alkaline massif (SP-MG, SE Brazil): relationships with the Serra do Mar analogues. Short Papers—IV South American Symposium on Isotope Geology, pp 593–595

Lyubetskaya T, Korenaga J (2007) Chemical composition of Earth's primitive mantle and its variance: 1 methods and results. J Geophys Res 112:B03211. doi:10.1019/2005JB004223

Machado DL (1991) Geologia e aspectos metalogenéticos do complexo alcalino-carbonatitico de Catalão II (GO), thèse. Universidade Estadual de Campinas (SP), Brésil, p 102

Mantovani MSM, Louro VHA, Ribeiro VB, Requejo HS, dos Santos RPZ (2016) Geophysical analysis of Catalão I alkaline–carbonatite complex in Goiás, Brazil. Geophys Prospec 36:216–227

Matteini M, Junges SL, Dantes EL, Pimentel MM, Bühn B (2010) In situ zircon U-Pb and Lu–Hf isotope systematic on magmatic rocks: insights on the crustal evolution of the Neoproterozoic Goiás Magmatic Arc, Brasília belt, Central Brazil. Gondwana Res 17:1–12

McFarlane CRM, McCulloch MT (2007) Coupling of in situ Sm–Nd systematics and U-Pb dating of monazite and allanite with applications to crustal evolution studies. Chem Geol 245:45–60

Melluso L, Lustrino M, Ruberti E, Brotzu P, Gomes CB, Morbidelli L, Morra V, Svisero DP, d'Amelio F (2008) Major- and trace-element composition of olivine, perovskite, clinopyroxene, Cr-Fe-Ti oxides, phlogopites and host kamafugites and kimberlites, Alto Paranaíba, Brazil. Can Miner 46:19–40

Melluso L, Srivastava RK, Guarino V, Zanetti A, Sinha AK (2010) Mineral compositions and magmatic evolution of the Sung Valley ultramafic-alkaline-carbonatitic complex (NE India). Can Miner 48:205–229

Melluso L, Srivastava RK, Petrone CM, Guarino V, Sinha AK (2012) Mineralogy and magmatic affinity of the Jasra clinopyroxenitic- gabbroic- syenitic complex, Shillong Plateau, northeastern India. Miner Mag 76(5):1099–1117

Melluso L, Morra V, Guarino V, De' Gennaro R, Franciosi L, Grifa C (2014) The crystallization of shoshonitic to peralkaline trachyphonolitic magmas in a H_2O-Cl-F-rich environment at Ischia (Italy), with implications for the feeder system of the Campania Plain volcanoes. Lithos 210–211:242–259

Melluso L, Guarino V, Lustrino M, Morra V, De' Gennaro R (2016) The REE- and HFSE-bearing phases in the Itatiaia alkaline complex (Brazil), and geochemical evolution of feldspar-rich felsic melts. Miner Mag in press. doi:10.1180/minmag.2016.080.122

Mitchell RH (2005) Carbonatites and carbonatites and carbonatites. Can Miner 43:2049–2068

Morbidelli L, Gomes CB, Beccaluva L, Brotzu P, Conte AM, Ruberti E, Traversa G (1995) Mineralogical, petrological and geochemical aspects of alkaline and alkaline-carbonatite associations from Brazil. Earth Sci Rev 39:135–168

Morbidelli L, Gomes CB, Beccaluva L, Brotzu P, Garbarino C, Riffel BF, Ruberti E, Traversa G (1997) Parental magma characterization of Salitre cumulate rocks (Alto Paranaíba Alkaline Province, Brazil) as inferred from mineralogical, petrographic, and geochemical data. Int Geol Rev 39:723–743

Morel MLA, Nebel O, Nebel-Jacobsen YJ, Miller JS, Vroon PZ (2008) Hafnium isotope characterization of the GJ-1 zircon reference material by solution and laser-ablation MC-ICPMS. Chem Geol 255:231–235

Nowell GM, Pearson DG, Irving AJ (2003a) Lu–Hf and Re–Os systematics of lamproites: constraints on their petrogenesis. Geophys Res Abstr 5:05458

Nowell GM, Pearson DG, Jacob DJ, Spetsius ZV, Nixon PH, Haggerty SE (2003b) The origin of alkremites and related rocks: a Lu–Hf, Rb–Sr and Sm–Nd isotope study. Extended abstracts 8th international kimberlite conference, victoria, extended abstracts, FLA 0271

Nowell GM, Pearson DG, Bell DR, Carlson RW, Smith CB, Kempton PD, Noble SR (2004) Hf isotope systematics of kimberlites and their megacrysts: new constraints on their source regions. J Petrol 45:1583–1612

Otto JW, Wyllie PJ (1993) Relationships between silicate melts and carbonate-precipitating melts in CaO–MgO–SiO_2–CO_2–H_2O at 2 kbar. Miner Petrol 48:343–365

Peucat J-J, Salomão J, Barbosa F, de Araújo Pinho IC, Paquette J-L, Martin H, Fanning M, de Menezes Leal AB, Cruz S (2011) Geochronology of granulites from the south Itabuna-Salvador-Curaçá Block, São Francisco Craton (Brazil): nd isotopes and U-Pb zircon ages. J South Am Earth Sci 31:397–413

Pimentel MM, Fuck RA, Silva JLH (1996) Dados Rb–Sr e Sm–Nd da região de Jussara-Goiás-Mossamedes (GO), e o limite entre terrenos antigos do Maciço de Goiás e o Arco Magmático de Goiás. Rev Bras Geociencias 26:61–70

Pimentel MM, Fuck RA, Gioia SMCL (2000) The Neoproterozoic Goiás magmatic arc, central Brazil: a review and new Sm–Nd isotopic data. Rev Bras Geociencias 30:35–39

Pouchou JL, Pichoir F (1988) A simplified version of the "PAP" model for matrix corrections in EPMA. In: Newbury DE (ed) Microbeam analysis. San Francisco Press, San Francisco, pp 315–318

Ramos FC, Wolff JA, Tollstrup DL (2004) Measuring $^{87}Sr/^{86}Sr$ variation in minerals and groundmass from basalts using LA–MC–ICPMS. Chem Geol 211:135–158

Read G, Grutter H, Winter S, Luckman N, Gaunt F, Thomsen F (2004) Stratigraphic relations, kimberlite emplacement and lithospheric thermal evolution, Quiricò Basin, Minas Gerais State, Brazil. Lithos 77:803–818

Riccomini C, Velazquez VF, Gomes CB (2005) Tectonic controls of the Mesozoic and Cenozoic alkaline magmatism in the central-southeastern Brazilian Platform. In: Comin-Chiaramonti P,

Gomes CB (eds) Mesozoic to Cenozoic alkaline magmatism in the Brazilian Platform. FAPESP, São Paulo, pp 31–55

Rocha E, Nasraoui M, Soubiès F, Bilal E, Perseval P (2001) Évolution géochimique du pyrochlore au cours de l'altération météorique du gisement de Catalão II (Goiás, Brésil). C Rend Ac Sci 332:91–98

Rossetti F, Tecce F, Billi A, Brilli M (2007) Patterns of fluid flow in the contact aureole of the Late Miocene Monte Capanne pluton (Elba Island, Italy): the role of structures and rheology. Contrib Miner Petrol 153:743–760

Ruberti E, Gomes CB, Comin-Chiaramonti P (2005) The alkaline magmatism from the Ponta Grossa Arch. In: Comin-Chiaramonti P, Gomes CB (eds) Mesozoic to Cenozoic alkaline magmatism in the Brazilian Platform. EDUSP/FAPESP, São Paulo, pp 473–521

Sato K, Tassinari CCG, Kawashita K, Petronilho L (1995) O método Geocronológico Sm-Nd no IG/USP e suas Aplicações. Anais Acad Brasil Ciências 67:313–336

Scherer E, Münker C, Mezger K (2006) Calibration of the lutetium–hafnium clock. Science 293:683–687

Sgarbi PBA, Heaman LM, Gaspar JC (2004) U-Pb perovskite ages for Brazilian kamafugitic rocks: further support for a temporal link to a mantle plume hotspot track. J South Am Earth Sci 16:715–724

Sharp ZD (1990) In situ laser microprobe techniques for stable isotope analysis. Chem Geol 101:3–19

Sonoki IK, Garda GM (1988) Idades K/Ar de rochas alcalinas do Brasil meridional e Paraguai oriental: compilação e adaptação às novas constantes de decaimento. Bol Inst Geoci USP, Série Científica 19:63–85

Stacey JS, Kramers JD (1975) Approximation of terrestrial lead isotope evolution by a two-stage model. Earth Planet Sci Lett 26:207–221

Tappe S, Foley SF, Jenner GA, Kjarsgaard BA (2005) Integrating ultramafic lamprophyres into the IUGS classification of igneous rocks: rational and implications. J Petrol 46:1893–1900

Tappe S, Foley SF, Stracke A, Romer RL, Kjarsgaard BA, Heaman LM, Joyce N (2007) Craton reactivation on the Labrador Sea margins: $^{40}Ar/^{39}Ar$ age and Sr–Nd– Hf–Pb isotope constraints from alkaline and carbonatite intrusives. Earth Planet Sci Lett 256:433–454

Tappe S, Foley SF, Kjarsgaard BA, Romer RL, Heaman LM, Stracke A, Jenner GA (2008) Between carbonatite and lamproite - diamondiferous Torngat ultramafic lamprophyres formed by carbonate-fluxed melting of cratonic MARID-type metasomes. Geochim Cosmochim Acta 72(13):3258–3286

Tappe S, Pearson DG, Nowell GM, Nielsen TFD, Milstead P, Muehlenbachs K (2011) A fresh isotopic look at Greenland kimberlites: cratonic mantle lithosphere imprint on deep source signal. Earth Planet Sci Lett 305:235–248

Tappe S, Pearson DG, Kjarsgaard BA, Nowell GM, Dowall D (2013) Mantle transition zone input to kimberlite magmatism near a subduction zone: origin of anomalous Nd–Hf isotope systematics at Lac de Gras, Canada. Earth Planet Sci Lett 371–372:235–251

Tappe S, Kjarsgaard BA, Kurszlaukis S, Nowell GM, Phillips D (2014) Petrology and Nd-Hf isotope geochemistry of the Neoproterozoic Amon Kimberlite Sills, Baffin Island (Canada): evidence for deep mantle magmatic activity linked to supercontinent cycles. J Petrol 55:2003–2042

Taylor HP Jr (1978) Water/rock interactions and origin of H_2O in granitic batholiths. J Geol Soc London 133:509–558

Taylor HP Jr, Frechen J, Degens ET (1967) Oxygen and carbon isotope studies of carbonatites from the Laacher See District, West Germany and the Alnö District, Sweden. Geochim Cosmochim Acta 31:407–430

Thompson RN, Gibson SA, Mitchell JG, Dickin AP, Leonardos OH, Brod JA, Greenwood JC (1998) Migrating Cretaceous-Eocene magmatism in the Serra do Mar Alkaline Province, SE Brazil: melts from the deflected Trindade mantle plume? J Petrol 39:1493–1526

Thomsen TB, Schmidt MW (2008) Melting of carbonated pelites at 2.5–5.0 GPa, silicate-carbonatite liquid immiscibility, and potassium-carbon metasomatism of the mantle. Earth Planet Sci Lett 267:17–31

Traversa G, Barbieri M, Beccaluva L, Coltorti M, Conte AM, Garbarino C, Gomes CB, Macciotta G, Morbidelli L, Ronca S, Scheibe LF (1996) Mantle sources and differentiation of alkaline magmatic suite of Lages, Santa Catarina, Brazil. Eur J Miner 8:193–208

Traversa G, Gomes CB, Brotzu P, Buraglini N, Morbidelli L, Principato MS, Ronca S, Ruberti E (2001) Petrography and mineral chemistry of carbonatites and mica-rich rocks from the Araxá complex (Alto Paranaíba Province, Brazil). Anais Acad Brasil Ciências 73:71–98

van Achterbergh E, Ryan C, Jackson S, Griffin W (2001) Appendix 3, data reduction software for LA–ICP–MS. In: Sylvester P (ed) Laser-Ablation–ICPMS in the Earth Sciences. Short Course Series vol 29. Mineral Association of Canada, pp 239–243

Vervoort JD, Patchett PJ, Soderlund U, Baker M (2004) Isotopic composition of Yb and the determination of Lu concentrations and Lu/Hf ratios by isotopic dilution using MC–ICPMS. Geochem Geophys Geosyst 5:Q11002. doi:10.1029/2004GC000721

Vroon PZ, van der Wagt B, Koornneef JM, Davies GR (2008) Problems in obtaining precise and accurate Sr isotope analysis from geological materials using laser ablation MC–ICPMS. Anal Bioanal Chem 390:465–476

Walter MJ, Bulanova GP, Armstrong LS, Keshav S, Blundy JD, Gudfinnsson G, Lord OT, Lennie AR (2008) Primary carbonatite melt from deeply subducted oceanic crust. Nature 454:622–625

Wasserburg GJ, Jacobsen SB, DePaolo DJ, McCulloch MT, Wen T (1981) Precise determination of Sm/Nd ratios, Sm and Nd isotopic abundances in standard solutions. Geochem Cosmochim Acta 45:2311–2323

Wenzel T, Baumgartner LP, Brugmann GE, Konnikov EG, Kislov EY (2002) Partial melting and assimilation of dolomitic xenoliths by mafics magma: the ioko-Dovyren intrusion (North Baikal Region, Russia). J Petrol 49(11):2049–2074

Woolley AR, Kempe DRC, Woolley AR (1989) Carbonatites: nomenclature, average chemical compositions and element distribution. In: Woolley AR, Kempe DRC (eds) Carbonatites: genesis and evolution. Unwin Hyman, London

Woolley AR, Kjarsgaard BA (2008a) Paragenetic types of carbonatite as indicated by the diversity and relative abundances of associated silicate rocks: evidence from a global database. Can Miner 46:741–752

Woolley AR, Kjarsgaard BA (2008b) Carbonatite occurrences of the world: Map and database. Geol Survey Canada Open File 5796

Wu FY, Yang YH, Xie LW, Yang JH, Xu P (2006) Hf isotopic compositions of the standard zircons and baddeleyites used in U-Pb geochronology. Chem Geol 234:105–126

Wu FY, Yang YH, Bulakh AG, Bellatreccia F, Mitchell RH, Li QL (2010a) In situ U-Pb and Nd–Hf–(Sr) isotopic investigations of zirconolite and calzirtite. Chem Geol 277:178–195

Wu FY, Yang YH, Mitchell RH, Li QL, Yang JH, Zhang YB (2010b) In situ U–Pb age determination and Nd isotopic analysis of perovskites from kimberlites in southern Africa and Somerset Island, Canada. Lithos 115:205–222

Wu FY, Arzamastsev AA, Mitchell RH, Li QL, Sun J, Yang YH, Wang RC (2013) Emplacement age and Sr–Nd isotopic compositions of the Afrikanda alkaline ultramafic complex, Kola Peninsula, Russia. Chem Geol 353:210–229

Wyatt BA, Baumgartner M, Anckar E, Grutter H (2004) Compositional classification of "kimberlitic" and "non-kimberlitic" ilmenite. Lithos 77:819–840

Wyllie PJ, Lee WJ (1998) Model system controls on conditions for formation of magnesiocarbonatite and calciocarbonatite magmas from the mantle. J Petrol 39:1885–1893

Xie LW, Zhang YB, Zhang HH, Sun JF, Wu FY (2008) In situ simultaneous determination of trace elements, U-Pb and Lu–Hf isotopes in zircon and baddeleyite. Chinese Sci Bull 53:1565–1573

Yang YH, Sun JF, Xie LW, Fan HR, Wu FY (2008) In situ Nd isotopic measurements of geological samples by laser ablation. Chinese Sci Bull 53:1062–1070

Yang YH, Wu FY, Wilde SA, Liu XM, Zhang YB, Xie LW, Yang JH (2009) In situ perovskite Sr-Nd isotopic constraints on the petrogenesis of the Ordovician Mengyin kimberlites in the North China Craton. Chem Geol 264:24–42

Yaxley GM, Green DH (1996) Experimental reconstruction of sodic dolomitic carbonatite melts from metasomatised lithosphere. Contrib Miner Petrol 124:359–369